J. Fluid Mech. (2005), *vol.* 523, *pp.* 121–159.
DOI: 10.1017/S0022112004002034 Printed in the United Kingdom

Mach wave radiation of nonlinearly evolving supersonic instability modes in shear layers

By XUESONG WU[1,2]

[1]Department of Mechanics, Tianjin University, P. R. China

[2]Department of Mathematics, Imperial College London, 180 Queens Gate, London SW7 2BZ, UK

(Received 21 December 2003 and in revised form 1 September 2004)

Shear flows at sufficiently high Mach numbers support instability waves which travel supersonically relative to the ambient free stream. Such supersonic modes are known to produce intense far-field sound in the form of Mach wave radiation. In this paper, the nonlinear evolution of supersonic modes and the associated Mach wave radiation are analysed in a self-consistent fashion by using the high-Reynolds-number matched asymptotic expansion in conjunction with the multiple-scale method. Attention is focused on the relatively weak disturbances for which the nonlinear effect is comparable with the non-parallel-flow effect. The nonlinear spatial development of the mode is described by an amplitude equation in which the nonlinear term is contributed by the critical layer. The directivity of the radiated Mach waves in the far field is determined explicitly in terms of the amplitude function. The analysis is applicable to plane mixing layers, boundary layers, and planar and circular jets. In particular, it is shown that for the last two flows, the radiated Mach waves are most intensive in a beam which is perpendicular to the Mach wave front and emanates from the streamwise position at which the instability mode attains its maximum amplitude. The theoretical results are compared with direct numerical simulation and experimental data, and favourable qualitative and quantitative agreement is obtained.

1. Introduction

Noise generated by unsteady hydrodynamic motion, such as jets, mixing layers or boundary layer flows, has long been a serious concern for numerous technology applications, in particular for the aviation industry. The principal theoretical approach to this fundamental problem in fluid mechanics has been the acoustic analogy of Lighthill (1952, 1954) and its various variants (e.g. Phillips 1960; Lilley 1974; Howe 1975). That approach is based on re-arranging the Navier–Stokes equations governing compressible flows to a form such that the left-hand-side operator apparently describes the 'propagation' of a sound wave, while the right-hand side may be interpreted as the effective 'source' acting on a fictitious acoustic medium. In the original formulation of Lighthill, the wave operator was taken to be the simplest possible, that for a uniform medium at rest, while the right-hand-side 'source' term was expressed in terms of a stress tensor, T_{ij}. A formal 'solution' to the wave equation can be written down for the density fluctuation ρ, in terms of a volume integral over the source region. This in essence amounts to an integral equation because the source term also contains the unknown density. Nevertheless this formal solution has been explored to gain useful information about the sound produced in the case where something about the nature of the source is known *a priori*.

In the low-Mach-number limit ($M \ll 1$), the characteristic acoustic wavelength is much larger than the domain of the hydrodynamics motion which contributes to the sound. In this case, Lighthill (1952) suggested that the density variation (i.e. compressibility) within the source region may be neglected, that is, the source term may be approximated by the fluctuating velocities corresponding to an incompressible flow field. Crow (1970) on the other hand approached the problem of sound radiation of low-Mach-number flows using systematic matched asymptotic expansions, and found that prediction of radiated sound requires some prior knowledge about the far-field asymptotic behaviour of the source. The convergence of Lighthill's quadrupole-form solution, obtained by exchanging the order of integration and differentiation, relies on a certain (far-field) property of T_{ij}. When the inevitable step of approximating T_{ij}, by $T_{ij}^{(0)}$ say, is taken, the required property may not always be guaranteed. Moreover, the sound produced by the neglected part ($T_{ij} - T_{ij}^{(0)}$) depends not only on size but also on its asymptotic behaviour of the latter, and may not necessarily be negligible. Therefore despite its apparent simplicity, it is not self-evident that Lighthill's approximation is equivalent to the leading-order asymptotic solution to the radiated sound. Such an equivalence has been established only in some special cases, e.g. sound radiation by a purely inviscid vorticity field in an infinite domain (see e.g. Kambe 1986).

In fully compressible shear flows, the acoustic wavelength is typically comparable with the shear-layer thickness, and consequently identification or approximation of the relevant sources becomes more problematic. Especially for supersonic flows, sound radiation exhibits features distinct from those of low-speed flows; see the review of Tam (1995) and recent experiments of Panda & Seasholtz (2002). One of them is that fluctuations which propagate supersonically relative to the ambient free stream radiate noise as highly directional Mach waves. This mechanism was first investigated by Phillips (1960). Instead of Lighthill's analogy, Phillips derived a convected acoustic wave equation which includes the effects of convection and refraction caused by the variation of the local mean speed of sound. The main source was attributed to velocity fluctuation, or more precisely to the product of the gradients of the fluctuating and mean velocities. Phillips (1960) obtained the large-M asymptotic solution, which indicates that the radiated sound of a given frequency and wavenumber may be associated with the source properties at the critical level. Using this solution in conjunction with a plausible assumption on the spectrum of velocity fluctuations, Phillips estimated that the radiated sound intensity scales as $M^{3/2}$, as oppose to the well-known M^8-law for low-Mach-number flows.

Ffowcs Williams & Maidanik (1965) took a somewhat different line of attack from that of Phillips (1960). They started from Lighthill's (1952) formal (exact) solution, and using the momentum equations manipulated the source term to a form consisting of, *inter alia*, the product of the density fluctuation ρ and the mean velocity gradient. They argued that this term would be the dominant source in the case of the mean velocity gradient exceeding the fluctuating velocity gradient. The density in the source was then related to the pressure fluctuation p using a 'local isentropic condition'. After several further steps of a conjectural nature and employing the empirical formula for the r.m.s. of $(\partial p/\partial t)^2$, they obtained a formula which correlates the radiated sound with the surface pressure. The prediction was found to be in good agreement with the measurements.

As was indicated above, the Navier–Stokes equations can be re-arranged in different ways to facilitate acoustic analogies, each having a different 'source term'. All of the

formulations would be equivalent, had the effective 'source' terms been evaluated exactly. However, some approximations have to be made to the source beforehand† in order to deduce any meaningful information about the radiated sound, and then the precise relation between, and the relative merits of, the different analogies become far from evident. Physically speaking, emission of sound waves occurs as a result of hydrodynamic fluctuations changing their character to become acoustic as they approach the far field. Since the acoustic analogy does not consider this physical process in detail, the choice of what constitutes the noise source and what constitutes the propagation effect was rather a subjective one, based on some intuitive reasoning rather than a systematic analysis. This is the case with the two aforementioned theoretical treatments of Mach wave radiation. In the work of Ffowcs Williams & Maidanik (1965), the refraction of the density fluctuation by the mean-flow gradient is taken to be the dominant source, while in Phillips (1960) it is taken to be a propagation effect. Experimental investigations of compressible jets (e.g. Panda & Seasholtz 2002) show that the acoustic spectrum and intensity in the far field are strongly correlated to those of the density fluctuation within the jet, suggesting that the latter is an important source.

Rather than investigating Mach wave radiation by general turbulent fluctuations, for which little quantitative information is available, Tam & Burton (1984*a*, *b*) focus on the Mach wave generated by the so-called supersonic instability modes, whose phase velocity exceeds the sound speed in the ambient stream. The instability wave is assumed to be of sufficiently small amplitude that it evolves linearly, i.e. it amplifies exponentially, attenuates and finally decays due to the gradual spreading of the shear flow. The entire process can be described by local quasi-parallel linear instability theory. The asymptotic expansion for hydrodynamic motion, however, breaks down in the far field (cf. Tam & Morris 1980), and thus an outer region needs to be introduced to accommodate the radiated Mach wave. The intensity of the latter is determined by matching with the inner expansion. The absolute intensity can be determined once the amplitude of the instability wave is prescribed, which was done by fitting with experimental data.

The idea that instability waves, or in a broader sense large-scale orderly structures, constitute a dominant source of noise goes back to Tam (1971), Bishop, Ffowcs Williams & Smith (1971) and Crow & Champagne (1971), among others. In the case of supersonic jets, the role of supersonic modes in radiating Mach waves was confirmed by a series of experiments in circular (McLaughlin, Morrison & Troutt 1975; Troutt & McLaughlin 1982) as well as elliptic (Kinzie & McLaughlin 1995) jets. Tam & Burton (1984*a*, *b*) applied their theory to the experimental conditions of Troutt & McLaughlin (1982), and showed that the predicted acoustic directivity agreed with the measurements quite well. In these experiments the Reynolds numbers were fairly low and the instability waves were introduced in a controlled manner. Flows of technological interest usually have much higher Reynolds numbers so that the flow field tends to be intrinsically more disorganized, and moreover naturally occurring instability waves would have a broadband spectrum.

† For instance, one of the latest approaches is to model the (complete) source term appearing in an acoustic analogy by assuming a parameterized spectral function with the parameters being determined by a steady flow computation using averaged equations of motion (e.g. Khavaran, Bridges & Freund 2002).

Mitchell, Lele & Moin (1997) were the first to compute the Mach waves radiated by small-amplitude (i.e. linear) axisymmetric supersonic modes by direct numerical simulations (DNS) in a domain sufficiently large to encompass the far field. The directivity and intensity of the sound predicted by DNS were found to be in good agreement with the theoretical results of Tam & Burton (1984*a*, *b*). In addition, Mitchell *et al.* (1997) demonstrated that Lighthill's acoustic analogy may be used to construct the sound field provided that the density fluctuation is retained in the stress tensor and the non-compactness of the source is taken into account; this is expected since the exact source (apart from linearization, which is justified because of small amplitude) was used in Lighthill's formulation which is exact. Avital, Sandham & Luo (1998) examined the Mach wave field of a temporally evolving mixing layer, using a variation of Tam & Burton's formulation as well as Phillips' (1960) acoustic analogy. Freund, Lele & Moin (2000) simulated a Mach 1.92 turbulent jet initiated by a turbulent inflow, and showed that the acoustic field exhibits a highly directional pattern that is characteristic of Mach waves. Mohseni, Colonius & Freund (2002) carried out simulations based on linearized Navier–Stokes equations for the same inflow condition as in Freund *et al.* (2000), and compared the outcome with the DNS result. They demonstrate that the Mach wave field is dominated by axisymmetric and first helical modes. In particular, the directivity of the Mach wave field appears to be accounted for well by the first helical modes, but its intensity was appreciably underestimated by the linearized approximation. This result implies that nonlinear effects may be important in Mach wave radiation. An obvious nonlinear effect is that associated with the growth and decay of supersonic instability modes. All these simulations were conducted at quite low Reynolds numbers.

During the last two decades or so, considerable advances were made in developing nonlinear instability theory of nearly parallel shear flows. It is now well-understood that as an initially linear instability mode evolves downstream, the nonlinear effect first becomes important in the critical layer. The subsequent nonlinear evolution can be described in a self-consistent fashion in the framework of the nonlinear critical-layer approach. The reader is referred to Goldstein (1994, 1995) and Cowley & Wu (1994) for reviews of this field. In compressible shear flows the nonlinear development of a single oblique mode has been investigated by Goldstein & Leib (1988) and Leib (1991). The latter paper is particularly relevant for the present work as it considers supersonic modes. Leib & Lee (1995) studied pairs of oblique waves, and found that their evolution was governed by the same amplitude equation as in the incompressible case (Goldstein & Choi 1989; Wu, Lee & Cowley 1993).

The aim of the present paper is to investigate the Mach wave radiation by supersonic instability waves or more generally wavetrains that undergo nonlinear development. In § 2, the problem is formulated first for a plane mixing layer. Attention will be focused on the regime in which nonlinear and non-parallel effects are of importance simultaneously. The nonlinear evolution of a planar supersonic mode is considered in § 3. By analysing the nonlinear interaction within the critical layer, an amplitude equation of Landau–Stuart type is derived. The Mach wave field radiated by this nonlinearly evolving mode is studied in § 4. It is shown the intensity and directivity can be expressed explicitly in terms of the amplitude. In § 5, the analysis is modified to predict the Mach wave radiated by axisymmetric and helical modes in a circular jet. Results of parametric studies are presented in § 6, where the theoretical predictions in the linear limit are compared with the relevant DNS and experimental data. A brief summary is given in § 7.

2. Formulation

To fix ideas, we consider a plane mixing layer, which forms between two oncoming streams of velocity U_1^* and U_2^* ($U_1^* > U_2^*$). The coordinates (x, y) are non-dimensionalized by δ^*, the thickness of the shear layer at a streamwise location of interest. The time t, the velocity (u, v) and the pressure p are non-dimensionalized by δ^*/U^*, U^* and R^*U^{*2} respectively, where $U^* = (U_1^* - U_2^*)/2$. The temperature, density, and viscosity (thermal diffusivity), non-dimensionalized by their respective values in the faster stream T^*, R^* and μ^* (κ^*), are denoted by θ, ρ and μ (κ). Both μ and κ depend on temperature, i.e. $\mu = \mu(\theta)$ and $\kappa = \kappa(\theta)$.

The velocity profile of the shear flow is given by

$$(\bar{U}(y, x_3), R^{-1}\bar{V}(y, x_3)) \quad \text{with} \quad x_3 = x/R,$$

where the Reynolds number R is defined as

$$R = R^*U^*\delta^*/\mu^*,$$

and will be assumed to be large in the present paper. The temperature and density profiles are denoted by $\bar{T}$ and $\bar{R}$ respectively, with $\bar{R} = 1/\bar{T}$. We define the Mach number

$$M = U^*/a^*$$

with a^* being the sound speed in the fast stream.

A linear instability analysis (e.g. Jackson & Grosch 1989) shows that at sufficiently high Mach numbers, a mixing layer supports two supersonic modes which propagate downstream supersonically relative to the fast and slow streams respectively. A supersonic instability mode amplifies until it reaches the neutral position $x_3 = x_{3,n}$, after which the mode decays. The neutral position is of special interest for three reasons. First, when approaching $x_{3,n}$, the instability wave is no longer confined within the shear layer, but becomes radiative instead, i.e. its amplitude is oscillatory and remains finite rather than decaying to zero in the free stream. In other words, the supersonic instability mode is locally in resonance with a Mach wave. Second, with the instability mode attaining its maximum magnitude on a linear basis and the emergence of a critical layer, the nonlinear effect, though negligible sufficiently upstream, is likely to become significant in the vicinity of $x_{3,n}$ according to nonlinear critical layer theory (Goldstein 1994, 1995; Cowley & Wu 1995). Third, as the linear growth rate diminishes, the no-parallel-flow effect becomes important in the region where $(x_3 - x_{3,n}) \sim O(R^{-1/2})$, i.e.

$$x_3 = x_{3,n} + R^{-1/2}\bar{x} \quad \text{with} \quad \bar{x} = O(1). \tag{2.1}$$

In this vicinity, the length scale over which the growth rate varies is comparable with the reciprocal of the growth rate (i.e. the length scale over which the amplitude evolves). The local mean velocity and temperature profiles can be approximated, to the required order, by

$$(\bar{U}(y, x_3), \bar{T}(y, x_3)) \approx (\bar{U}(y, x_{3,n}), \bar{T}(y, x_{3,n})) + R^{-1/2}(\bar{U}_1(y), \bar{T}_1(y))\bar{x}.$$

In the following, unless otherwise stated $\bar{U}$ and $\bar{T}$ are to be understood to stand for $\bar{U}(y, x_{3,n})$ and $\bar{T}(y, x_{3,n})$ respectively.

The primary interest of the present paper is to predict Mach wave radiation as a supersonic mode evolves nonlinearly. The dominant nonlinear effect comes from the critical layer, and may come into play in different fashions depending on the form of disturbance and its initial amplitude. In the present study, we consider the relatively

weak disturbance, for which nonlinearity becomes significant in the region as specified by (2.1), producing an effect comparable with the non-parallelism. The $O(R^{-1/2})$ non-equilibrium effect associated with the slow modulation is then much smaller than the viscous effect, and hence the critical layer is viscosity dominated and has a width of $O(R^{-1/3}\delta^*)$. For simplicity, we start with a two-dimensional wave, for which it is found that the threshold magnitude

$$\epsilon = O\left(R^{-11/12}\right). \tag{2.2}$$

A disturbance with $\epsilon \ll R^{-11/12}$ would evolve through $x_{3,n}$ without being affected by nonlinearity. On the other hand, if $\epsilon \gg R^{-11/12}$, the location where the nonlinear effect becomes important shifts upstream. A new distinct regime arises when $\epsilon = O(R^{-5/6})$, for which the critical layer becomes non-equilibrium as well as viscous. The nonlinear development in this regime of a single supersonic instability mode was studied by Leib (1991). The disturbance evolves over a length scale of $O(R^{2/5}\delta^*)$, which is much shorter than the $O(R^{1/2}\delta^*)$ scale so that the non-parallel flow effect is negligible to leading order. The amplitude equation derived by Leib (1991) describes the nonlinear evolution in a region located at an $O(R^{3/5}\delta^*)$ distance upstream. It does not, however, describe how the disturbance evolves through the neutral position. Before one could predict the Mach wave radiation of such a relatively strong instability mode, it is necessary first to construct a composite solution which is uniformly valid over the $O(R^{1/2}\delta^*)$ length scale and capable of describing the growth and decay of the disturbance. Such a task is left for further investigation; the present study is concerned with the disturbance with the characteristic amplitude (2.2), which the evolves nonlinearly in the region specified by (2.1).

In practice, the disturbances usually have a broadband spectrum. Even in controlled experiments where an instability mode of a specific frequency is excited, the resulting disturbance would consist of a narrow band of spectral components centred at the frequency of excitation (see e.g. figure 16 of Troutt & McLaughlin 1982). A disturbance of this type corresponds to a wavetrain which modulates simultaneously in time and space. In the present analysis, the wavetrain is allowed to modulate on the $O(R^{-1/2})$ time scale so that it can be conveniently described by assuming that its amplitude depends on the slow time variable

$$\bar{t} = R^{-1/2}t,$$

as well as on the spatial variable $\bar{x}$.

3. Nonlinear evolution of supersonic instability modes

The development of the instability mode of interest is described by a double-layered structure consisting of the main layer, where the unsteady flow is linear and inviscid to the required order, and the critical layer, where both nonlinear and viscous effects are important.

3.1. *Main layer*

In the main layer, where $y = O(1)$, the disturbance expands as

$$(u, v, p, \theta, \rho) = \epsilon\left[A(\bar{x}, \bar{t})(\hat{u}_0, \hat{v}_0, \hat{p}_0, \hat{\theta}_0, \hat{\rho}_0) + R^{-1/2}(\hat{u}_1, \hat{v}_1, \hat{p}_1, \hat{\theta}_1, \hat{\rho}_1)\right]E + \text{c.c.} + \cdots \tag{3.1}$$

where $E = \mathrm{e}^{\mathrm{i}\alpha(x-ct)}$ describes the carrier wave with α and c being the wavenumber and phase speed respectively. $A(\bar{x}, \bar{t})$ is the amplitude function of the wavetrain. Such

a wavetrain consists of spectral components of $O(R^{-1/2})$ bandwidth centred at the frequency of the carrier wave.

Substitution of (3.1) into the compressible Navier–Stokes equations yields the continuity, energy and momentum equations for the disturbance

$$\left.\begin{aligned} &\mathrm{i}\alpha(\bar{U}-c)\hat{\rho}_0+\bar{R}'\hat{v}_0+\bar{R}(\mathrm{i}\alpha\hat{u}_0+\hat{v}_0')=0,\\ &\mathrm{i}\alpha(\bar{U}-c)\hat{\theta}_0+\bar{T}'\hat{v}_0=\mathrm{i}\alpha(\gamma-1)M^2(\bar{U}-c)\bar{T}\hat{p}_0,\\ &\mathrm{i}\alpha(\bar{U}-c)\hat{u}_0+\bar{U}'\hat{v}_0=-\mathrm{i}\alpha\bar{T}\hat{p}_0,\\ &\mathrm{i}\alpha(\bar{U}-c)\hat{v}_0=-\bar{T}\hat{p}_0', \end{aligned}\right\} \tag{3.2}$$

where γ stands for the ratio of specific heats, and a prime denotes a derivative with respect to y. The system (3.2) is supplemented by the state equation for a perfect gas, which expands as

$$1+\gamma M^2\hat{p}_0=\bar{R}\hat{\theta}_0+\bar{T}\hat{\rho}_0.$$

Eliminating $\hat{u}_0$, $\hat{v}_0$, $\hat{\rho}_0$ and $\hat{\theta}_0$ leads to the familiar compressible Rayleigh equation for the leading-order pressure $\hat{p}_0$:

$$\mathscr{L}\hat{p}_0\equiv\left\{\frac{\partial^2}{\partial y^2}+\left(\frac{\bar{T}'}{\bar{T}}-\frac{2\bar{U}'}{(\bar{U}-c)}\right)\frac{\partial}{\partial y}-\alpha^2\left(1-\frac{M^2(\bar{U}-c)^2}{\bar{T}}\right)\right\}\hat{p}_0=0. \tag{3.3}$$

Let $\bar{U}_\pm$ and $\bar{T}_\pm$ denote the velocity and temperature in the free streams. Then as $y\to\pm\infty$,

$$\hat{p}_0\sim\mathscr{C}_\infty^\pm\,\mathrm{e}^{\mathrm{i}q_\pm y}\quad\text{with}\quad q_\pm=\alpha\left(\frac{M^2(\bar{U}_\pm-c)^2}{\bar{T}_\pm}-1\right)^{1/2}$$

where the branch cuts are taken to ensure that the disturbance is an outgoing wave, and $\mathscr{C}_\infty^\pm$ are constants that can be determined by normalization of the eigenfunction. For a general growing supersonic mode, its eigenfunction $\hat{p}_0$ decays exponentially as $y\to\pm\infty$. However, at the neutral location $x_{3,n}$, α and c are both real and hence $\hat{p}_0$ is finite, exhibiting a sinusoidal wave behaviour at ∞ or $-\infty$, provided

$$|c-\bar{U}_\pm|>T_\pm^{1/2}/M\equiv c_\pm. \tag{3.4}$$

This implies that in the vicinity of the neutral position, the energy of a supersonic instability mode radiates to the far field in the form of a Mach wave, if the disturbance propagates relative to the free stream at a speed larger than the ambient sound speed $c_\pm$. This is expected on the basis of the familiar wavy-wall analogy. In the present situation, because condition (3.4) is satisfied only close to $x_{3,n}$, the apparent source of radiation would appear to be localized. The wavy-wall analogy cannot provide any information about the character of the directivity of the acoustic field.

Let y_c denote the critical level, at which $\bar{U}(y_c)-c=0$. It was shown by Leib (1991) that as $\eta\equiv y-y_c\to0$,

$$\hat{p}_0\sim\frac{\bar{U}_c'}{\bar{T}_c}\left\{\frac{\alpha^2}{3}a^\pm\phi_a+\phi_b+\frac{\alpha^2}{3}\left(\frac{\bar{T}_c'}{\bar{T}_c}-\frac{\bar{U}_c''}{\bar{U}_c'}\right)\ln|\eta|\phi_a\right\}, \tag{3.5}$$

where the subscript c signifies a quantity evaluated at y_c, and

$$\left.\begin{aligned} &\phi_a\sim\eta^3+\chi_a\eta^4+\cdots,\\ &\phi_b\sim1-\tfrac{1}{2}\alpha^2\eta^2+\chi_b\eta^4+\cdots, \end{aligned}\right\} \tag{3.6}$$

with

$$\chi_a = -\frac{3}{4}\left(\frac{\bar{T}'}{\bar{T}} - \frac{\bar{U}''}{\bar{U}'}\right),$$

$$\chi_b = \frac{\alpha^2}{4}\left\{\frac{\bar{T}_c''}{\bar{T}_c} - \left(\frac{\bar{T}_c'}{\bar{T}_c}\right)^2 + \tfrac{1}{2}\left(\frac{\bar{U}_c''}{\bar{U}_c'}\right)^2 - \frac{2}{3}\frac{\bar{U}_c'''}{\bar{U}_c'} - \frac{M^2\bar{U}_c'^2}{\bar{T}_c} - \frac{\alpha^2}{2} + \frac{11}{12}\left(\frac{\bar{T}'}{\bar{T}} - \frac{\bar{U}''}{\bar{U}'}\right)^2\right\}.$$

It follows from the y-momentum and energy equations in (3.2) that as $\eta \to 0$,

$$\hat{v}_0 \sim -\mathrm{i}\alpha\left\{1 - \left(\frac{\bar{T}_c'}{\bar{T}_c} - \frac{\bar{U}_c''}{\bar{U}_c'}\right)\eta\ln|\eta| + \left(\frac{2}{3}\frac{\bar{T}_c'}{\bar{T}_c} - \frac{1}{6}\frac{\bar{U}_c''}{\bar{U}_c'} - a^{\pm}\right)\eta + \cdots\right\},$$

$$\hat{\theta}_0 \sim \frac{\bar{T}_c'}{\bar{U}_c'\eta}.$$

The logarithmic singularity in $\hat{p}_0$ arises because the critical level of a supersonic mode does not coincide the generalized inflection point. The temperature perturbation exhibits the familiar singularity of a simple-pole form. The dominant nonlinear effect in the critical layer is associated with these two singularities.

At the next order, it can be shown that $\hat{p}_1$ satisfies the inhomogeneous Rayleigh equation

$$\mathscr{L}\hat{p}_1 = \frac{2\mathrm{i}c}{\alpha}\frac{\partial A}{\partial \bar{x}}\left\{\frac{\bar{U}'\hat{p}_0'}{(\bar{U}-c)^2} + \frac{\alpha^2}{c}\left[\frac{M^2\bar{U}(\bar{U}-c)}{\bar{T}} - 1\right]\hat{p}_0\right\} + \frac{2\mathrm{i}}{\alpha}\frac{\partial A}{\partial \bar{t}}\left\{\frac{\bar{U}'\hat{p}_0'}{(\bar{U}-c)^2} + \frac{\alpha^2 M^2(\bar{U}-c)\hat{p}_0}{\bar{T}}\right\} - \bar{x}A\Delta_1, \quad (3.7)$$

where

$$\Delta_1 = \left\{\frac{2\bar{U}'}{\bar{U}-c}\left(\frac{\bar{U}_1}{\bar{U}-c} - \frac{\bar{U}_1'}{\bar{U}'}\right) + \frac{T'}{T}\left(\frac{\bar{T}_1'}{\bar{T}'} - \frac{\bar{T}_1}{\bar{T}}\right)\right\}\hat{p}_0' + \alpha^2 M^2\frac{(\bar{U}-c)^2}{\bar{T}}\left(\frac{2\bar{U}_1}{\bar{U}-c} - \frac{\bar{T}_1}{\bar{T}}\right)\hat{p}_0.$$

It can be shown that

$$\hat{p}_1 \sim y\,\mathrm{e}^{\mathrm{i}q_{\pm}y} \quad \text{as} \quad y \to \pm\infty,$$

implying that the expansion (3.1) becomes disordered when $y \sim R^{1/2}$. On the other hand, as $y \to y_c$,

$$\hat{p}_1 \sim \frac{\alpha^2}{\bar{T}_c}\left[\frac{\mathrm{i}}{\alpha}\left(\frac{\partial A}{\partial \bar{t}} + c\frac{\partial A}{\partial \bar{x}}\right) - \bar{U}_{1c}\bar{x}A\right]\left\{\eta - \left(\frac{\bar{T}_c'}{\bar{T}_c} - \frac{\bar{U}_c''}{\bar{U}_c'}\right)\eta^2\ln|\eta| - \left[a^{\pm} + \frac{1}{3}\left(\frac{\bar{T}_c'}{\bar{T}_c} - \frac{\bar{U}_c''}{\bar{U}_c'}\right)\right]\eta^2 + \frac{1}{3}j\,\eta^3\ln|\eta|\right\} + \frac{\bar{U}_c'}{\bar{T}_c}(\mathrm{i}\alpha A)\eta^2 + \left(\frac{\alpha^2\bar{U}_c'}{3\bar{T}_c}\bar{x}A\right)j_1\eta^3\ln|\eta| + c^{\pm}\phi_a + d\left[\phi_b + \frac{\alpha^2}{3}\left(\frac{\bar{T}_c'}{\bar{T}_c} - \frac{\bar{U}_c''}{\bar{U}_c'}\right)\ln|\eta|\phi_a\right], \quad (3.8)$$

where $c^{\pm}$ and d are arbitrary functions of $\bar{x}$, and

$$j = \frac{\bar{T}_c''}{\bar{T}_c} - \frac{\bar{U}_c'''}{\bar{U}_c'} - \left(\frac{\bar{T}_c'}{\bar{T}_c}\right)^2 + \left(\frac{\bar{U}_c''}{\bar{U}_c'}\right)^2 + 3\left(\frac{\bar{T}_c'}{\bar{T}_c} - \frac{\bar{U}_c''}{\bar{U}_c'}\right)^2 - 2\left(\frac{\bar{T}_c'}{\bar{T}_c} - \frac{\bar{U}_c''}{\bar{U}_c'}\right)\frac{\bar{U}_c'}{\bar{U}_c},$$

$$j_1 = \frac{\bar{T}_c'}{\bar{T}_c}\left(\frac{\bar{T}_{1c}'}{\bar{T}_c'} - \frac{\bar{T}_{1c}}{\bar{T}_c}\right) + \frac{\bar{U}_c''}{\bar{U}_c'}\left(\frac{\bar{U}_{1c}'}{\bar{U}_c'} - \frac{\bar{U}_{1c}''}{\bar{U}_c''}\right) - 2\left(\frac{\bar{T}_c'}{\bar{T}_c} - \frac{\bar{U}_c''}{\bar{U}_c'}\right)\frac{\bar{U}_{1c}}{\bar{U}_c}.$$

In order for the inhomogeneous system (3.7) to have an acceptable solution, it has to satisfy a solvability condition. The latter can be derived by multiplying both sides of (3.7) by $\bar{T}/(\bar{U}-c)^2\hat{p}_0$ and integrating from $-\infty$ and ∞, leading to

$$-\frac{1}{\bar{U}_c'}\left\{3(c^+-c^-)-2\frac{\alpha^2}{\bar{T}_c}\left[\frac{\mathrm{i}}{\alpha}\left(\frac{\partial A}{\partial \bar{t}}+c\frac{\partial A}{\partial \bar{x}}\right)-\bar{U}_{1c}\bar{x}A\right]\left(\frac{\bar{T}_c'}{\bar{T}_c}-\frac{\bar{U}_c''}{\bar{U}_c'}\right)(a^+-a^-)\right.$$
$$\left.-\alpha^2 d(a^+-a^-)\right\}=\frac{2\mathrm{i}}{\alpha}\left[cI_2\frac{\partial A}{\partial \bar{x}}+I_3\frac{\partial A}{\partial \bar{t}}\right]-(\bar{x}A)I_1, \quad (3.9)$$

where

$$I_1=\int_{-\infty}^{\infty}\left\{\left[\frac{2\bar{U}'}{\bar{U}-c}\left(\frac{\bar{U}_1}{\bar{U}-c}-\frac{\bar{U}_1'}{\bar{U}'}\right)+\frac{T'}{T}\left(\frac{\bar{T}_1'}{\bar{T}'}-\frac{\bar{T}_1}{\bar{T}}\right)\right]\frac{\bar{T}\hat{p}_0\hat{p}_0'}{(\bar{U}-c)^2}+\alpha^2M^2\left(\frac{2\bar{U}_1}{\bar{U}-c}-\frac{\bar{T}_1}{\bar{T}}\right)\hat{p}_0^2\right\}\mathrm{d}y,$$
$$I_2=\int_{-\infty}^{\infty}\left\{\frac{\bar{T}\bar{U}'\hat{p}_0\hat{p}_0'}{(\bar{U}-c)^4}+\frac{\alpha^2}{c}\left[\frac{M^2\bar{U}}{(\bar{U}-c)}-\frac{\bar{T}}{(\bar{U}-c)^2}\right]\hat{p}_0^2\right\}\mathrm{d}y,$$
$$I_3=\int_{-\infty}^{\infty}\left\{\frac{\bar{T}\bar{U}'\hat{p}_0\hat{p}_0'}{(\bar{U}-c)^4}+\frac{\alpha^2M^2\hat{p}_0^2}{\bar{U}-c}\right\}\mathrm{d}y;$$

these integrals are to be understood as finite parts in the sense of Hadamard. The jumps (a^+-a^-) and (c^+-c^-) will be derived by analysing the flow in the critical layer.

3.2. *Critical layer*

The solution in the main shear layer becomes singular at the critical level y_c. A separate solution must be constructed in a thin region surrounding y_c, where viscosity is introduced to remove the singularity. The dominant balance is therefore between the advection and viscous diffusion, and that determines the critical-layer width to be $O(R^{-1/3})$; so we introduce the local transverse variable

$$Y=(y-y_c)/R^{-1/3}. \quad (3.10)$$

The solution for the perturbation expands as

$$\left.\begin{aligned}
u&=\epsilon\left(U_1E+R^{-1/6}U_2E+R^{-1/4}U_M+R^{-1/2}U_3E\right)+\text{c.c.}+\cdots,\\
\theta&=\epsilon R^{1/3}\left(\Theta_1E+R^{-1/6}\Theta_2E+R^{-1/4}\Theta_M+R^{-1/2}\Theta_3E\right)+\text{c.c.}+\cdots,\\
v&=\epsilon\left(V_0E+R^{-1/3}V_1E+R^{-1/2}V_2E+R^{-7/12}V_M+R^{-5/6}V_3E\right)+\text{c.c.}+\cdots,\\
p&=\epsilon\left(P_0E+R^{-1/3}P_1E+R^{-1/2}P_2E+R^{-5/6}P_3E\right)+\text{c.c.}+\cdots.
\end{aligned}\right\} \quad (3.11)$$

Here $P_0=A\bar{U}_c'/\bar{T}_c$, and $V_0=-\mathrm{i}\alpha A$, which are simply the trivial continuations of the leading-order main-layer solution. Terms at logarithmic orders have not been written out explicitly since they automatically match with those in the outer solution. The expansion for the density of the perturbation, ρ, is omitted, since to the required order of approximation, ρ is related to the temperature θ via

$$\rho=-\frac{\theta}{\bar{T}_c^2}.$$

The leading-order term in the temperature expansion, $\tilde{\Theta}_1$, is governed by

$$\mathscr{L}_\kappa\Theta_1+\bar{T}_c'V_0=0,$$

where the operator $\mathscr{L}_\kappa$ is defined as

$$\mathscr{L}_\kappa = \mathrm{i}\alpha\bar{U}_c' Y - \bar{T}_c\kappa_c\frac{\partial^2}{\partial Y^2}. \tag{3.12}$$

The solution is found to be

$$\Theta_1 = (\mathrm{i}\alpha\bar{T}_c' A)\int_0^\infty \exp(-s_\kappa\xi^3 - \mathrm{i}\alpha\bar{U}_c' Y\xi)\,\mathrm{d}\xi, \quad \text{with} \quad s_\kappa = \tfrac{1}{3}(\alpha\bar{U}_c')^2\bar{T}_c\kappa_c. \tag{3.13}$$

Expansion of the continuity and x-momentum equations yields

$$\mathrm{i}\alpha\bar{U}_c' Y\left(-\Theta_1/\bar{T}_c^2\right) + \frac{1}{\bar{T}_c}(\mathrm{i}\alpha U_1 + V_{1,Y}) - \frac{\bar{T}_c'}{\bar{T}_c^2}V_0 = 0,$$

$$\mathscr{L}_\mu U_1 + \bar{U}_c' V_1 + \bar{U}_c'' Y V_0 = -\mathrm{i}\alpha\bar{T}_c P_1 - \bar{T}_c' Y(\mathrm{i}\alpha)P_0 + \bar{T}_c\mu_c'\bar{U}_c'\frac{\partial\Theta_1}{\partial Y},$$

where $\mathscr{L}_\mu$ is the same as $\mathscr{L}_\kappa$ provided that μ_c replaces κ_c in (3.12). The above two equations can be combined to obtain

$$\mathscr{L}_\mu U_{1,Y} = \bar{U}_c'(\bar{T}_c\mu_c' - \kappa_c)\Theta_{1,YY} - \mathrm{i}\alpha\bar{U}_c'\left(\frac{\bar{T}_c'}{\bar{T}_c} - \frac{\bar{U}_c''}{\bar{U}_c'}\right)A + \cdots,$$

where we have ignored the terms which do not contribute to the jump. The solution is found to be

$$\begin{aligned} U_{1,Y} = {} & (\mathrm{i}\alpha\bar{U}_c' A)\frac{\bar{T}_c'(\bar{T}_c\mu_c' - \kappa_c)}{\bar{T}_c(\mu_c - \kappa_c)}\int_0^\infty [1 - \exp(-(s_\kappa - s)\xi^3)]\exp(-s\xi^3 - \mathrm{i}\alpha\bar{U}_c' Y\xi)\,\mathrm{d}\xi \\ & - (\mathrm{i}\alpha\bar{U}_c' A)\left(\frac{\bar{T}_c'}{\bar{T}_c} - \frac{\bar{U}_c''}{\bar{U}_c'}\right)\int_0^\infty \exp(-s\xi^3 - \mathrm{i}\alpha\bar{U}_c' Y\xi)\,\mathrm{d}\xi, \end{aligned} \tag{3.14}$$

with $s = \frac{1}{3}(\alpha\bar{U}_c')^2\bar{T}_c\mu_c$. Matching U_1 with its outer counterpart determines the jump

$$a^+ - a^- = \left(\frac{\bar{T}_c'}{\bar{T}_c} - \frac{\bar{U}_c''}{\bar{U}_c'}\right)\pi\mathrm{i}. \tag{3.15}$$

The nonlinear interaction of the wave at the quadratic order generates a first harmonic as well as a mean-flow distortion, but only the latter influences the evolution of the wave; so we shall consider this component only. It follows from the energy equation that

$$\bar{T}_c\kappa_c\frac{\partial^2\Theta_M}{\partial Y^2} = V_0\frac{\partial\Theta_1^*}{\partial Y}, \tag{3.16}$$

and hence

$$\Theta_{M,Y} = -\frac{\alpha^2\bar{T}_c'}{\bar{T}_c\kappa_c}|A|^2\int_0^\infty \exp(-s_\kappa\xi^3 + \mathrm{i}\alpha\bar{U}_c' Y\xi)\,\mathrm{d}\xi.$$

The continuity and x-momentum equations at this order give

$$\frac{1}{\bar{T}_c}\frac{\partial V_M}{\partial Y} = \frac{V_0}{\bar{T}_c^2}\frac{\partial\Theta_1^*}{\partial Y}, \tag{3.17}$$

$$\bar{U}_c' V_M - \bar{T}_c\mu_c\frac{\partial^2 U_M}{\partial Y^2} = -V_0\frac{\partial U_1^*}{\partial Y} - (\mathrm{i}\alpha P_0)\Theta_1^* + \bar{T}_c\mu_c'\bar{U}_c'\Theta_{M,Y}. \tag{3.18}$$

Equations (3.16) and (3.17) indicate that

$$V_M = \kappa_c\Theta_{M,Y},$$

which is inserted into (3.18), to give

$$U_{M,YY} = -\frac{\alpha^2 \bar{U}_c' \bar{T}_c' (\bar{T}_c \mu_c' - \kappa_c)}{\bar{T}_c^2 \mu_c (\mu_c - \kappa_c)} |A|^2 \int_0^\infty [\exp(-(s - s_\kappa)\xi^3) - s/s_\kappa] \exp(-s_\kappa \xi^3 + \mathrm{i}\alpha \bar{U}_c' Y \xi)\, \mathrm{d}\xi$$
$$+ \frac{\alpha^2 \bar{U}_c'}{\bar{T}_c \mu_c} \left(\frac{\bar{T}_c'}{\bar{T}_c} - \frac{\bar{U}_c''}{\bar{U}_c'} \right) |A|^2 \int_0^\infty \exp(-s\xi^3 + \mathrm{i}\alpha \bar{U}_c' Y \xi)\, \mathrm{d}\xi$$
$$+ \frac{\alpha^2 \bar{U}_c' \bar{T}_c'}{\bar{T}_c^2 \mu_c} |A|^2 \int_0^\infty \exp(-s_\kappa \xi^3 + \mathrm{i}\alpha \bar{U}_c' Y \xi)\, \mathrm{d}\xi. \tag{3.19}$$

The jump $(c^+ - c^-)$ can be calculated by considering $(U_3, V_3, \Theta_3, P_3)$, which satisfy the equations

$$\mathscr{L}_\mu U_3 + \bar{U}_c' V_3 = -\mathrm{i}\alpha \bar{T}_c P_3 - V_0 U_{M,Y} - (\mathrm{i}\alpha P_0)\Theta_M + \bar{T}_c \mu_c' \bar{U}_c' \Theta_{3,Y} + \cdots, \tag{3.20}$$

$$\mathrm{i}\alpha \bar{U}_c' Y \left(-\Theta_3 / \bar{T}_c^2\right) + \frac{1}{\bar{T}_c}(\mathrm{i}\alpha U_3 + V_{3,Y}) = \frac{V_0}{\bar{T}_c^2} \Theta_{M,Y} + \cdots, \tag{3.21}$$

$$\mathscr{L}_\kappa \Theta_3 = -V_0 \Theta_{M,Y} + \cdots. \tag{3.22}$$

Here we have retained only the terms associated with the fundamental interacting with the mean-flow distortion, which will contribute the nonlinear part of the jump $(c^+ - c^-)$. The linear inhomogeneous terms have not been included since they contribute to the linear part of $(c^+ - c^-)$. That part corresponds to the familiar $(-\pi)$ phase jump across the critical layer of the logarithmic singularity in the outer solution, and so can be easily written out. In order to calculate the nonlinear part of the jump, equation (3.22) is solved first to obtain

$$\Theta_3 = -\frac{\mathrm{i}\alpha^3 \bar{T}_c'}{\bar{T}_c \kappa_c} A |A|^2 \int_0^\infty \int_0^\infty \exp[-2s_\kappa \xi^3 + s_\kappa (\xi - \eta)^3 + \mathrm{i}\alpha \bar{U}_c' (\xi - \eta) Y]\, \mathrm{d}\xi\, \mathrm{d}\eta. \tag{3.23}$$

Equations (3.20) and (3.21) can be reduced to

$$\mathscr{L}_\mu U_{3,Y} = -V_0 U_{M,YY} - (\mathrm{i}\alpha P_0)\Theta_{M,Y} + \bar{U}_c' (\bar{T}_c \mu_c' - \kappa_c)\Theta_{3,YY} + \cdots,$$

which is then solved by using Fourier transform. Matching U_3 with the outer solution determines the jump

$$c^+ - c^- = \frac{1}{3} \frac{\alpha^2}{\bar{T}_c} \left[\frac{\mathrm{i}}{\alpha} \left(\frac{\partial A}{\partial \bar{t}} + c \frac{\partial A}{\partial \bar{x}} \right) - \bar{U}_{1c} \bar{x} A \right] j\pi\mathrm{i} + \left(\frac{\alpha^2 \bar{U}_c'}{3 \bar{T}_c} \bar{x} A \right) j_1 \pi\mathrm{i}$$
$$+ d \frac{\alpha^2}{3} \left(\frac{\bar{T}_c'}{\bar{T}_c} - \frac{\bar{U}_c''}{\bar{U}_c'} \right) \pi\mathrm{i} + \frac{\Lambda}{3} A |A|^2, \tag{3.24}$$

where

$$\Lambda = \frac{\pi \alpha^4 \bar{U}_c'^2}{3 \bar{T}_c^2 \mu_c} \left\{ \frac{\bar{T}_c' (\bar{T}_c \mu_c' - \kappa_c)}{\bar{T}_c (\mu_c - \kappa_c)} \left(\left(\frac{\mu_c}{\kappa_c} \right)^{4/3} - 1 \right) + \left(\frac{\bar{T}_c'}{\bar{T}_c} - \frac{\bar{U}_c''}{\bar{U}_c'} \right) \right.$$
$$\left. + \frac{\bar{T}_c'}{\bar{T}_c} \left(1 + \frac{\mu_c}{\kappa_c} \right)^{2/3} \left(\frac{2\mu_c}{\kappa_c} \right)^{1/3} \right\} (2s)^{-1/3} \Gamma\left(\tfrac{1}{3}\right). \tag{3.25}$$

3.3. *Amplitude equation and solution*

Inserting the jumps (3.15) and (3.24) into (3.9), we obtain the amplitude equation for A:

$$\frac{\partial A}{\partial \bar{x}} + c_g^{-1} \frac{\partial A}{\partial \bar{t}} = \sigma \bar{x} A + l A |A|^2, \tag{3.26}$$

where

$$c_g = cG \Big/ \left\{ 2I_3 + \frac{\alpha^2}{\bar{T}_c \bar{U}'_c} \left[j - 2\left(\frac{\bar{T}'_c}{\bar{T}_c} - \frac{\bar{U}''_c}{\bar{U}'_c} \right)^2 \right] \pi \mathrm{i} \right\},$$

$$\sigma = (-\mathrm{i}\alpha/c) \left\{ I_1 + \frac{\alpha^2}{\bar{T}_c} \left[\frac{\bar{U}_{1c}}{\bar{U}'_c} \left(j - 2\left(\frac{\bar{T}'_c}{\bar{T}_c} - \frac{\bar{U}''_c}{\bar{U}'_c} \right)^2 \right) - j_1 \right] \pi \mathrm{i} \right\} \Big/ G,$$

$$l = \mathrm{i}\alpha \Lambda / (c \bar{U}'_c G),$$

with

$$G = 2I_2 + \frac{\alpha^2}{\bar{T}_c \bar{U}'_c} \left[j - 2\left(\frac{\bar{T}'_c}{\bar{T}_c} - \frac{\bar{U}''_c}{\bar{U}'_c} \right)^2 \right] \pi \mathrm{i}.$$

Note that because the group velocity c_g is complex, the usual idea of describing a wavepacket in a coordinate travelling with c_g is inapplicable (cf. Stewartson & Stuart 1971). Thus, the appropriate evolution equation is of first order as opposed to the familiar Schrödinger type of equation.

If A is independent of $\bar{t}$, the disturbance consists of a pure tone and will be referred to as a simple or single wave. In this case, the appropriate initial condition for the evolution equation (3.26) is

$$A \to a_0 \, \mathrm{e}^{\sigma \bar{x}^2/2} \quad \text{as} \quad \bar{x} \to -\infty \tag{3.27}$$

so that the nonlinear solution matches to the linear stage upstream. Here the constant a_0 is a measure of the initial amplitude, and it can be taken to be real without loss of generality. Equation (3.26) can be solved analytically to give

$$|A|^2 = a_0^2 \, \mathrm{e}^{\sigma_r \bar{x}^2} \left[1 - 2 l_r a_0^2 \int_{-\infty}^{\bar{x}} \mathrm{e}^{\sigma_r \xi^2} \, \mathrm{d}\xi \right]^{-1}, \tag{3.28}$$

where σ_r and l_r stand for the real parts of σ and l respectively, with $\sigma_r < 0$ as expected. The nature of the solution depends on l_r and a_0. If $l_r < 0$, nonlinearity has a stabilizing effect and the amplitude grows first and then ultimately decays to zero for all values of a_0. However if $l_r > 0$, the amplitude goes through amplification followed by decay only when a_0 is below a threshold value a_c, with a_c determined by

$$a_c^2 = \frac{1}{2 l_r} \sqrt{\frac{-\sigma_r}{\pi}}. \tag{3.29}$$

For $a_0 > a_c$, the solution develops a singularity at a finite distance $\bar{x}_c$, with $\bar{x}_c$ determined by

$$2 l_r a_0^2 \int_{-\infty}^{\bar{x}_c} \mathrm{e}^{\sigma_r \xi^2} \, \mathrm{d}\xi = 1.$$

For the general modulation case, it is convenient to consider the solution for A in the spectral space. Let $\widehat{A}(\bar{x}, \tilde{\omega})$ denote the Fourier transform of A with respect to $\bar{t}$. Then the Fourier transform of (3.26) becomes

$$\widehat{A}'(\bar{x}, \tilde{\omega}) = \left(\sigma \bar{x} - \mathrm{i} c_g^{-1} \tilde{\omega} \right) \widehat{A} + \frac{l}{(2\pi)^2} \int_{-\infty}^{\infty} \int_{-\infty}^{\infty} \widehat{A}(\tilde{\omega} - \tilde{\omega}_1) \widehat{A}(\tilde{\omega}_2) \widehat{A}^*(\tilde{\omega}_2 - \tilde{\omega}_1) \, \mathrm{d}\tilde{\omega}_2 \, \mathrm{d}\tilde{\omega}_1. \tag{3.30}$$

It is to be solved subject to the initial condition

$$\widehat{A}(\bar{x}, \tilde{\omega}) \to a_s(\tilde{\omega}) \exp\left(\tfrac{1}{2} \sigma \bar{x}^2 - \mathrm{i} c_g^{-1} \tilde{\omega} \bar{x} \right) \quad \text{as} \quad \bar{x} \to -\infty. \tag{3.31}$$

Obviously this again follows from the requirement of matching to the linear stage upstream, during which the disturbance has a spectrum $a_s(\tilde{\omega})$, with each component evolving independently. To be specific, we shall consider

$$a_s(\tilde{\omega}) = a_0 \, \mathrm{e}^{-\Delta|\tilde{\omega}|}, \tag{3.32}$$

where a_0 and Δ are two parameters measuring the overall intensity and the envelope time scale of the wavepacket respectively. Alternatively in the spectral space, Δ^{-1} represents the spectral bandwidth of the wavepacket. A simple wave can be viewed as the limiting case $\Delta \gg 1$.

4. Mach wave radiation

4.1. *Near field of Mach waves*

As was noted earlier, a neutral supersonic mode is oscillatory without exhibiting attenuation on the length scale of $y = O(1)$. Thus significant perturbations persist outside the shear layer. These perturbations represent the Mach waves, the character of which is the focus of this section. As will be shown, the Mach wave field consists of two distinct regions. The first corresponds to $y \sim R^{-1/2}$, and it is suggested by the fact that the main-deck expansion (3.1) becomes disordered when $y \sim R^{1/2}$. (A similar breakdown occurs in the case of an instability mode evolving on a subsonic shear flow (Tam & Morris 1980)). To describe the wave modulation in this region, which will be referred to as the near field of the Mach waves, we introduce the variable

$$\bar{y} = R^{-1/2} y. \tag{4.1}$$

The solution for the perturbation, the pressure p say, must be a function of x, y, t, $\bar{x}\,\bar{y}$ and $\bar{t}$, i.e.

$$p = p(x, y, t; \bar{x}, \bar{y}, \bar{t}).$$

Note that since the disturbance exhibits wave character in both x- and y-directions, the envelope modulations in these two directions are treated on an equal footing by simultaneously introducing the two slow variables $\bar{x}$ and $\bar{y}$.

In each stream, the perturbation expands as

$$(\boldsymbol{u}, p, \theta, \rho) = \epsilon \left[(\boldsymbol{u}_0, p_0, \theta_0, \rho_0) + R^{-1/2}(\boldsymbol{u}_1, p_1, \theta_1, \rho_1) + R^{-1}(\boldsymbol{u}_2, p_2, \theta_2, \rho_2) + \cdots \right]. \tag{4.2}$$

The perturbation is governed by Euler equations linearized about the uniform background flow $(\bar{U}_\pm, \bar{T}_\pm, \bar{R}_\pm)$. At leading order, they are

$$\left.\begin{aligned}
&\left(\frac{\partial}{\partial t} + \bar{U}_\pm \frac{\partial}{\partial x}\right)\rho_0 + \frac{1}{\bar{T}_\pm}\nabla \cdot \boldsymbol{u}_0 = 0, \\
&\left(\frac{\partial}{\partial t} + \bar{U}_\pm \frac{\partial}{\partial x}\right)\boldsymbol{u}_0 = -\bar{T}_\pm \nabla p_0, \\
&\bar{R}_\pm \left(\frac{\partial}{\partial t} + \bar{U}_\pm \frac{\partial}{\partial x}\right)\theta_0 = (\gamma - 1)M^2 \left(\frac{\partial}{\partial t} + \bar{U}_\pm \frac{\partial}{\partial x}\right) p_0, \\
&\gamma M^2 p_0 = \bar{T}_\pm \rho_0 + \bar{R}_\pm \theta_0.
\end{aligned}\right\} \tag{4.3}$$

Elimination of $\boldsymbol{u}_0$, θ_0 and ρ_0 leads to the convected wave equation for the pressure p_0:

$$M_\pm^2 \left(\frac{\partial}{\partial t} + \bar{U}_\pm \frac{\partial}{\partial x}\right)^2 p_0 - \nabla^2 p_0 = 0 \quad \text{with} \quad M_\pm = M/\sqrt{\bar{T}_\pm}. \tag{4.4}$$

This equation has the characteristics

$$\zeta = x - ct + q_{\pm} y = \text{constant}, \quad q_{\pm} = [M_{\pm}^2(\bar{U}_{\pm} - c)^2 - 1]^{1/2}. \tag{4.5}$$

The appropriate solution consistent with the far-field asymptote of the main-deck solution takes the form

$$p_0(x, y, t; \bar{x}, \bar{y}) = \bar{p}_0(\bar{x}, \bar{y})\, \mathrm{e}^{\mathrm{i}\alpha\zeta} + \text{c.c.}, \tag{4.6}$$

where $\bar{p}_0$ represents the envelope of the Mach wave, and its functional form will be determined by considering p_1.

Proceeding to the next order, we find that

$$M_{\pm}^2\left(\frac{\partial}{\partial t} + \bar{U}_{\pm}\frac{\partial}{\partial x}\right)^2 p_1 - \nabla^2 p_1 = -2\left\{ M_{\pm}^2(\bar{U}_{\pm} - c)\frac{\partial}{\partial \bar{t}} + [M_{\pm}^2 \bar{U}_{\pm}(\bar{U}_{\pm} - c) - 1]\frac{\partial}{\partial \bar{x}} - q_{\pm}\frac{\partial}{\partial \bar{y}} \right\} \frac{\partial p_0}{\partial \zeta}. \tag{4.7}$$

The solution for p_1 would contain an unacceptable secular term proportional to ζ as $\zeta \to \infty$, unless the right-hand side is identically zero. Use of (4.6) at this condition yields

$$M_{\pm}^2(\bar{U}_{\pm} - c)\frac{\partial \bar{p}_0}{\partial \bar{t}} + \{M_{\pm}^2 \bar{U}_{\pm}(\bar{U}_{\pm} - c) - 1\}\frac{\partial \bar{p}_0}{\partial \bar{x}} - q_{\pm}\frac{\partial \bar{p}_0}{\partial \bar{y}} = 0, \tag{4.8}$$

while matching with the main-deck solution provides the boundary condition

$$\bar{p}_0(\bar{x}, \bar{y}, \bar{t}) = \mathscr{C}_{\infty}^{\pm} A(\bar{x}, \bar{t}) \quad \text{at} \quad \bar{y} = 0. \tag{4.9}$$

Equation (4.8) has characteristics

$$\left.\begin{aligned} \bar{\xi} &= \bar{x} + q_{\pm}^{-1}(M_{\pm}^2 \bar{U}_{\pm}(\bar{U}_{\pm} - c) - 1)\bar{y} = \text{constant}, \\ \bar{\eta} &= \bar{t} + M_{\pm}^2(\bar{U}_{\pm} - c) q_{\pm}^{-1} \bar{y} = \text{constant}, \end{aligned}\right\} \tag{4.10}$$

along which the envelope $\bar{p}_0$ is constant, i.e. $\bar{p}_0(\bar{x}, \bar{y}, \bar{t}) = \bar{p}_0(\bar{\xi}, \bar{\eta})$. Applying the boundary condition (4.9) then fully determines $\bar{p}_0$ as

$$\bar{p}_0(\bar{x}, \bar{y}, \bar{t}) = \mathscr{C}_{\infty}^{\pm} A(\bar{\xi}, \bar{\eta}). \tag{4.11}$$

Therefore, the radiated Mach wave in the near field, where $\bar{x}, \bar{y} \sim O(1)$, is determined explicitly in terms of the amplitude A:

$$p_0 = \mathscr{C}_{\infty}^{\pm} A(\bar{\xi}, \bar{\eta})\, \mathrm{e}^{\mathrm{i}\alpha\zeta} + \text{c.c.} \tag{4.12}$$

With this analytical result, the mechanism or process of Mach wave radiation by a supersonic instability wavetrain now becomes clear: a Mach wave is formed as a result of the phase of the supersonic wavetrain propagating along the characteristics $\zeta = \text{constant}$, while its envelope propagates along the characteristics $\bar{\xi} = \text{constant}$ and $\bar{\eta} = \text{constant}$. This is illustrated schematically in figure 1. The phase relation of the Mach wave fronts is as expected from the familiar wavy-wall analogy, but added is the crucial information about the envelope.

For the relatively weak disturbance considered here, its amplitude $A \to 0$ as $\bar{x} \to \pm\infty$. Suppose that A attains its maximum at $\bar{x}_s$, and then the radiated Mach wave is strongest along the line

$$\bar{x} + q_{\pm}^{-1}(M_{\pm}^2 \bar{U}_{\pm}(\bar{U}_{\pm} - c) - 1)\bar{y} = \bar{x}_s, \tag{4.13}$$

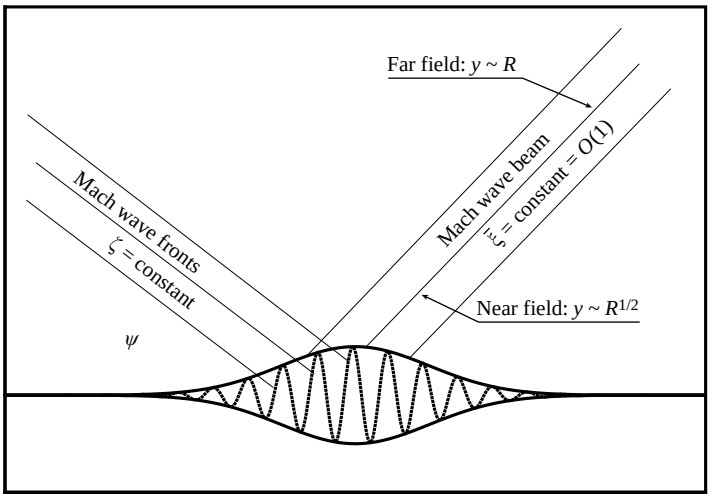

FIGURE 1. A sketch illustrating the radiation process and the structure of the Mach wave field.

and its energy concentrates in a region corresponding to $\bar{\xi} = O(1)$, which will be referred to as the Mach wave beam (see figure 1). Obviously, the direction of the beam depends on three parameters: the phase speed of the instability mode c, the mean velocity $\bar{U}_\pm$ of the ambient stream, and the jet Mach number $M_\pm$ based on the ambient sound speed. In particular for planar jets, $\bar{U}_\pm = 0$, and (4.13) reduces to

$$\bar{x} - \bar{y}/q_\pm = \bar{x}_s,$$

so that the Mach wave beam is perpendicular to the Mach wave front, and appears to emanate from the streamwise location where the amplitude of the instability mode is maximum.

The boundary-value problem (4.8)–(4.9) can alternatively be solved by Fourier transform with respect to $\bar{t}$ to give the solution

$$\bar{p}_0 = \mathscr{C}_\infty^\pm \int_{-\infty}^{\infty} \widehat{A}(\bar{\xi}, \tilde{\omega}) \exp\left[\mathrm{i}\frac{M_\pm^2}{q_\pm}(\bar{U}_\pm - c)\tilde{\omega}\bar{y} + \mathrm{i}\tilde{\omega}\bar{t}\right] \mathrm{d}\tilde{\omega} \equiv \mathscr{C}_\infty^\pm A(\bar{\xi}, \bar{\eta}),$$

where $\widehat{A}(\bar{\xi}, \tilde{\omega})$ is obtained by solving (3.30)–(3.31). The quantity of interest is the 'time average' of the acoustic power $\overline{\bar{p}_0^2}$, defined here as the integral of $\bar{p}_0^2$ from $-\infty$ to ∞ divided by Δ. It follows from the convolution theorem that

$$\overline{\bar{p}_0^2} = \frac{|\mathscr{C}_\infty^\pm|^2}{2\pi\Delta} \int_{-\infty}^{\infty} |\widehat{A}(\xi, \tilde{\omega})|^2 \, \mathrm{d}\tilde{\omega} \equiv |\mathscr{C}_\infty^\pm|^2 \overline{A(\xi, \bar{t})^2}. \tag{4.14}$$

Formulae (4.11) and (4.14) show that the Mach wave radiated by a wavepacket exhibits the same feature as that emitted by a single wave: the acoustic energy is conserved along the straight characteristic lines $\bar{\xi} = \text{constant}$.

4.2. *Far field of the Mach wave beam*

The analysis in §4.1 can be carried out to high orders. Consideration of p_2 leads to a secular condition for p_1, which in turn shows that $p_1 \sim \bar{y} A(\bar{\xi}, \bar{\eta})$, implying that expansion (4.2) breaks down when $\bar{y} \sim R^{1/2}$. The radiated Mach wave concentrates in the beam corresponding to $\bar{\xi} = O(1)$ with little wave activity outside this beam. In the following, we consider the solution in the far field of the Mach wave beam

(see figure 1), represented by

$$\bar{y} = O\left(R^{1/2}\right), \quad \bar{\xi} = O(1). \tag{4.15}$$

The appropriate variable is

$$\tilde{y} = R^{-1/2}\bar{y} = R^{-1}y, \tag{4.16}$$

and the expansion for the perturbation pressure now takes the form

$$p = [\tilde{p}_0(\bar{\xi}, \bar{\eta}, \tilde{y}) + R^{-1}\tilde{p}_1(\bar{\xi}, \bar{\eta}, \tilde{y}) + \cdots]\, \mathrm{e}^{\mathrm{i}\alpha\zeta} + \text{c.c.}$$

The secular condition for $\tilde{p}_1$ now becomes

$$2\mathrm{i}\alpha q_\pm \frac{\partial \tilde{p}_0}{\partial \tilde{y}} + q_\pm^{-2} M_\pm^2 \left\{ c^2 \frac{\partial^2 \tilde{p}_0}{\partial \bar{\xi}^2} + 2c \frac{\partial^2 \tilde{p}_0}{\partial \bar{\xi}\, \partial \bar{\eta}} + \frac{\partial^2 \tilde{p}_0}{\partial \bar{\eta}^2} \right\} = 0, \tag{4.17}$$

while matching with (4.11) imposes the boundary condition

$$\tilde{p}_0 = \mathscr{C}_\infty^\pm A(\bar{\xi}, \bar{\eta}) \quad \text{at} \quad \tilde{y} = 0. \tag{4.18}$$

For a simple wave, A is independent of $\bar{t}$ and hence of $\bar{\eta}$, and equation (4.17) then reduces to

$$2\mathrm{i}\alpha q_\pm \frac{\partial \tilde{p}_0}{\partial \tilde{y}} + q_\pm^{-2} M_\pm^2 c^2 \frac{\partial^2 \tilde{p}}{\partial \bar{\xi}^2} = 0, \tag{4.19}$$

which is a Schrödinger equation with $\tilde{y}$ playing the role of time in the conventional setting. Equation (4.19) can be solved as a heat equation through the substitution $\tilde{y} \to \mathrm{i}\tilde{y}$ and analytic continuation in the resulting solution.† The equation may alternatively be solved by Fourier transform with respect to $\bar{\xi}$. Either way the solution is found to be

$$\tilde{p}_0(\bar{\xi}, \tilde{y}) = \frac{\mathrm{e}^{-\pi\mathrm{i}/4}}{\sqrt{\tilde{y}}} \left(\frac{\alpha q_\pm^3}{2\pi M_\pm^2 c^2} \right)^{1/2} \mathscr{C}_\infty^\pm \int_{-\infty}^{\infty} A(\zeta) \exp\left\{ \frac{\mathrm{i}\alpha q_\pm^3}{2M_\pm^2 c^2 \tilde{y}} (\bar{\xi} - \zeta)^2 \right\} \mathrm{d}\zeta. \tag{4.20}$$

The full system (4.17)–(4.18) can be solved best by taking the Fourier transform with respect to $\bar{\eta}$. Then the Fourier transform of $\tilde{p}_0$, $\widehat{P}$, is found to be

$$\widehat{P}(\bar{\xi}, \tilde{\omega}, \tilde{y}) = \frac{\mathrm{e}^{-\pi\mathrm{i}/4}}{\sqrt{\tilde{y}}} \left(\frac{\alpha q_\pm^3}{2\pi M_\pm^2 c^2} \right)^{1/2} \mathscr{C}_\infty^\pm \widehat{Q}(\bar{\xi}, \tilde{\omega}, \tilde{y}) \exp\left\{ -\frac{\mathrm{i} M_\pm^2 \tilde{\omega}^2 \tilde{y}}{2\alpha q_\pm^3} \right\} \tag{4.21}$$

with

$$\widehat{Q}(\bar{\xi}, \tilde{\omega}, \tilde{y}) = \int_{-\infty}^{\infty} \widehat{A}(\zeta, \tilde{\omega}) \exp\left\{ \frac{\mathrm{i}\alpha q_\pm^3}{2M_\pm^2 c^2 \tilde{y}} \left(\bar{\xi} - \zeta + \frac{M_\pm^2 c \tilde{\omega} \tilde{y}}{\alpha q_\pm^3} \right)^2 \right\} \mathrm{d}\zeta. \tag{4.22}$$

For a wavetrain with a frequency bandwidth Δ^{-1}, the 'time averaged' acoustic power, as defined in the previous subsection, is given by

$$\overline{(\tilde{p}_0)^2} = \frac{1}{\tilde{y}} \left(\frac{\alpha q_\pm^3 |\mathscr{C}_\infty^\pm|^2}{4\pi^2 M_\pm^2 c^2 \Delta} \right) \int_{-\infty}^{\infty} |\widehat{Q}(\xi, \tilde{\omega}, \tilde{y})|^2 \, \mathrm{d}\tilde{\omega}. \tag{4.23}$$

In the far field of the Mach wave beam, acoustic energy is no longer conserved along the straight lines $\bar{\xi} = \text{constant}$, that is, the diffraction effect is now significant.

† The author is indebted to Dr John Gibbons for pointing this method out to him.

Thus far, we have shown that the Mach wave field is fully determined once the amplitude function A is known. It should be noted that although the analysis in this section (and also that of the forthcoming § 5.2) is presented for a wavetrain modulated on the particular time and length scales of $O(R^{1/2})$, it in fact can be easily recast for a wavetrain modulated on arbitrary slow scales.

The idea of matching an 'outer' acoustic field with an 'inner' hydrodynamic is a fundamental principle in the asymptotic approach to aeroacoustics. It has been employed by Tam & Morris (1980) and Crighton & Huerre (1990) to study sound waves radiated by a subsonically propagating instability wave. The present work shows that the acoustic field emitted by a supersonic mode has a quite different structure, and the analysis involved also differs considerably.

We end this section by contrasting the present approach with that of Tam & Burton (1984*a*, *b*). Apart from a linearly evolving supersonic mode being considered in their work, both studies used essentially the same basic idea of determining the Mach wave, i.e. by matching with the local hydrodynamic field. Here we are able to derive a more explicit result by taking advantage of the fact that the length scales characterizing the wavefront/phase and envelope of the Mach wave are asymptotically distinct. In seeking the solution for the Mach wave, Tam & Burton (1984*a*, *b*) did not exploit such a scale disparity, and as a result the solution had to be expressed in terms of a Fourier integral, which has to be evaluated numerically in order to see the nature of the Mach wave radiation, whereas the simple analytical result derived in the present paper provides an immediate characterization of the radiated Mach waves.

It is straightforward to adapt the analysis and results in this section to the analogous problem in boundary layers. In the rest of the paper, we shall consider a circular jet, which is one of the most important practical flows in which Mach wave radiation plays a significant part in noise generation.

5. Extension to a circular jet

For a circular jet, it is natural to use cylindric polar coordinates (x, r, θ). The velocity components in the axial, radial and azimuthal directions are denoted by (u, v, w). The exit nozzle radius R_J and the exit speed U_J will be taken as the reference length and velocity respectively so that the reference time is R_J/U_J. The density ρ and temperature θ are non-dimensionalized by the jet density ρ_J and temperature Θ_J, respectively. We define the Reynolds number and Mach number as

$$R = \rho_J U_J R_J/\mu_J, \quad M = U_J/c_J \tag{5.1}$$

where c_J is the sound speed at the jet exit.

The linear instability of supersonic jets has been a subject of extensive investigation (see e.g. Tam & Hu 1989; Luo & Sandham 1997 and references therein). Two families of supersonic instability modes have been identified: one is a continuation of the usual incompressible Kelvin–Helmholtz or Rayleigh instability, and the other comes into existence at some finite $M > 1$. The present concern is with modes in the first family as they appear to be a major source of supersonic jet noise (Tam, Chen & Seiner 1992), at least for relatively low Mach numbers. When such an instability mode is excited upstream, it will amplify until it approaches the neutral location $x_{3,n}$, after which it starts to decay. In the vicinity of $x_{3,n}$, part of the energy of the mode radiates to the far field, giving rise to a distinct Mach wave field (Troutt & McLaughlin 1982).

Experiments show that both axisymmetric and helical modes make appreciable contributions to the jet noise, and so we shall consider the disturbance which is

either an axisymmetric mode or a pair of helical modes with azimuthal wavenumbers $\pm m$. The helical modes with $m=\pm1$ are particularly important because they have the largest integral growth (Tam *et al.* 1992). It turns out that much of the analysis for both forms of disturbances can be treated on the same footing, although there exists a significant difference in their nonlinear critical-layer dynamics, which we shall highlight later in § 5.3.

5.1. *Main layer*

In the main deck, the disturbance expands as

$$(u, v, w, p, \theta, \rho) = \epsilon[A(\bar{x}, \bar{t})(\hat{u}_0, \hat{v}_0, \hat{w}_0, \hat{p}_0, \hat{\theta}_0, \hat{\rho}_0) + R^{-1/2}(\hat{u}_1, \hat{v}_1, \hat{w}_1, \hat{p}_1, \hat{\theta}_1, \hat{\rho}_1)]E\cos m\theta + \text{c.c.} + \cdots. \quad (5.2)$$

The axisymmetric mode appears as a special case with $m=0$. The threshold amplitude ϵ for nonlinear development depends on the form of the disturbances, and will be specified later. At the present stage, it suffices to mention that ϵ is sufficiently small that the perturbation in the main deck is linear to the required order of approximation. The governing equations, at leading order, are

$$\begin{aligned}
&\mathrm{i}\alpha(\bar{U}-c)\hat{\rho}_0 + \bar{R}'\hat{v}_0 + \bar{R}\left(\mathrm{i}\alpha\hat{u}_0 + \frac{\partial\hat{v}_0}{\partial r} + \frac{\hat{v}_0}{r} + \frac{m}{r}\hat{w}_0\right) = 0,\\
&\mathrm{i}\alpha(\bar{U}-c)\hat{u}_0 + \bar{U}'\hat{v}_0 = -\mathrm{i}\alpha\bar{T}\hat{p}_0,\\
&\mathrm{i}\alpha(\bar{U}-c)\hat{v}_0 = -\bar{T}\frac{\partial\hat{p}_0}{\partial r},\\
&\mathrm{i}\alpha(\bar{U}-c)\hat{w}_0 = \frac{\bar{T}m}{r}\hat{p}_0,\\
&\mathrm{i}\alpha(\bar{U}-c)\hat{\theta}_0 + \bar{T}'\hat{v}_0 = \mathrm{i}\alpha M^2(\gamma-1)(\bar{U}-c)\bar{T}\hat{p}_0.
\end{aligned}$$

On eliminating $\hat{u}_0$, $\hat{v}_0$, $\hat{w}_0$, $\hat{\rho}_0$ and $\hat{\theta}_0$ in favour of the pressure $\hat{p}_0$, we obtain

$$\left\{\frac{\partial^2}{\partial r^2} + \frac{1}{r}\frac{\partial}{\partial r} + \left(\frac{\bar{T}'}{\bar{T}} - \frac{2\bar{U}'}{\bar{U}-c}\right)\frac{\partial}{\partial r} + \left(\frac{\alpha^2M^2}{\bar{T}}(\bar{U}-c)^2 - \alpha^2 - \frac{m^2}{r^2}\right)\right\}\hat{p}_0 = 0. \quad (5.3)$$

It follows from the regularity requirement at $r=0$ that

$$\hat{p}_0 \sim \mathscr{C}_0\left(\frac{\nu r}{2}\right)^m\left[\frac{1}{m!} + \frac{(\nu r)^2}{4(m+1)!} + \cdots\right] \quad \text{as} \quad r\to 0, \quad (5.4)$$

where $\nu=\alpha[1-M^2(c-1)^2]^{1/2}$, Bessel function of order m, whilst and $\mathscr{C}_0$ is a constant to be determined by normalization of the eigenfunction.

In the ambient fluid, $\bar{U}\to 0$ and $\bar{T}\to T_a$ (constant), and it follows from (5.3) that as $r\to\infty$,

$$\hat{p}_0 \to \frac{\mathscr{C}_\infty}{\sqrt{r}}\,\mathrm{e}^{\mathrm{i}\alpha qr} \quad \text{with} \quad q=(M^2c^2/T_a-1)^{1/2}, \quad (5.5)$$

where T_a denotes the temperature of the ambient fluid, and constant $\mathscr{C}_\infty$ is to be fixed by normalization. Result (5.5) indicates that the mode is radiating if $c>T_a^{1/2}/M\equiv c_a$, i.e. if the instability wave travels faster than the ambient sound speed c_a.

In the vicinity of the critical level r_c, where $\bar{U}(r_c)-c=0$, $\hat{p}_0$ has the local asymptotic solution

$$\hat{p}_0 \sim \frac{\bar{U}_c'}{\bar{T}_c}\left\{\frac{\bar{\alpha}^2}{3}a^{\pm}\phi_a + \phi_b + \frac{\bar{\alpha}^2}{3}\widehat{k}\ln|\eta|\phi_a\right\}, \tag{5.6}$$

where $\eta \equiv r - r_c \ll 1$, and

$$\bar{\alpha} = \left(\alpha^2 + m^2/r_c^2\right)^{1/2}, \quad \widehat{k} = \left(\frac{\bar{T}_c'}{\bar{T}_c} - \frac{\bar{U}_c''}{\bar{U}_c'} + \frac{1}{r_c}\right) - \frac{2m^2}{\bar{\alpha}^2 r_c^3}.$$

The functions ϕ_a and ϕ_b are as given in (3.6) except that χ_a and χ_b are modified to

$$\chi_a = -\frac{3}{4}\left(\frac{\bar{T}_c'}{\bar{T}_c} - \frac{\bar{U}_c''}{\bar{U}_c'} + \frac{1}{r_c}\right),$$

$$\chi_b = \frac{1}{4}\left\{\bar{\alpha}^2\left[\frac{\bar{T}_c''}{\bar{T}_c} - \left(\frac{\bar{T}_c'}{\bar{T}_c}\right)^2 + \tfrac{1}{2}\left(\frac{\bar{U}_c''}{\bar{U}_c'}\right)^2 - \frac{2}{3}\frac{\bar{U}_c'''}{\bar{U}_c'} - \frac{1}{r_c^2} - \frac{\bar{\alpha}^2}{2} + \frac{11}{12}\left(\frac{\bar{T}_c'}{\bar{T}_c} - \frac{\bar{U}_c''}{\bar{U}_c'} + \frac{1}{r_c}\right)^2\right]\right.$$
$$\left. - \frac{\alpha^2 M^2 \bar{U}_c'^2}{\bar{T}_c} - \frac{11}{6}\left(\frac{\bar{T}_c'}{\bar{T}_c} - \frac{\bar{U}_c''}{\bar{U}_c'} + \frac{1}{r_c}\right)\frac{m^2}{r_c^3} + \frac{3m^2}{r_c^4}\right\}, \tag{5.7}$$

and the $(-\alpha^2/2)$ in ϕ_b is replaced by $(-\bar{\alpha}^2/2)$. For helical modes, the streamwise and spanwise velocity components both exhibit a singularity of a single-pole form at the critical level, i.e.

$$\hat{u}_0 \sim \left(\frac{m^2}{\alpha^2 r_c^2}\right)\frac{1}{\eta}, \qquad \hat{w}_0 \sim -\left(\frac{\mathrm{i}m}{\alpha r_c}\right)\frac{1}{\eta}. \tag{5.8}$$

It is easy to show that $\hat{p}_1$ is governed by an inhomogeneous Rayleigh equation with the same right-hand side as (3.7). It is found that as $\eta \to 0$,

$$\hat{p}_1 \sim \frac{\bar{\alpha}^2}{\bar{T}_c}\left[\frac{\mathrm{i}}{\alpha}\left(\frac{\partial A}{\partial \bar{t}} + c\frac{\partial A}{\partial \bar{x}}\right) - \bar{U}_{1c}\bar{x}A\right]\left\{\eta - \widehat{k}\eta^2\ln|\eta| - \left(a^{\pm} + \tfrac{1}{3}\widehat{k} + \frac{m^2}{\bar{\alpha}^2 r_c^3}\right)\eta^2 + \tfrac{1}{3}j\eta^3\ln|\eta|\right\}$$
$$+ \frac{\bar{U}_c'}{\bar{T}_c}(\mathrm{i}\alpha A')\eta^2 + \left(\frac{\bar{\alpha}^2\bar{U}_c'}{3\bar{T}_c}\bar{x}A\right)j_1\eta^3\ln|\eta| + c^{\pm}\phi_a + d\left[\phi_b + \frac{\bar{\alpha}^2}{3}\widehat{k}\ln|\eta|\phi_a\right], \tag{5.9}$$

where

$$\left.\begin{aligned} j &= \frac{\bar{T}_c''}{\bar{T}_c} - \frac{\bar{U}_c'''}{\bar{U}_c'} - \left(\frac{\bar{T}_c'}{\bar{T}_c}\right)^2 + \left(\frac{\bar{U}_c''}{\bar{U}_c'}\right)^2 - \frac{1}{r_c^2} + 3\left(\frac{\bar{T}_c'}{\bar{T}_c} - \frac{\bar{U}_c''}{\bar{U}_c'} + \frac{1}{r_c}\right)^2 \\ &\quad - \frac{2\alpha^2}{\bar{\alpha}^2}\left(\frac{\bar{T}_c'}{\bar{T}_c} - \frac{\bar{U}_c''}{\bar{U}_c'} + \frac{1}{r_c}\right)\frac{\bar{U}_c'}{\bar{U}_c} - \frac{2m^2}{\bar{\alpha}^2 r_c^3}\left[2\left(\frac{\bar{T}_c'}{\bar{T}_c} - \frac{\bar{U}_c''}{\bar{U}_c'} + \frac{1}{r_c}\right) - \frac{3}{r_c}\right], \\ j_1 &= \frac{\bar{T}_c'}{\bar{T}_c}\left(\frac{\bar{T}_{1c}'}{\bar{T}_c'} - \frac{\bar{T}_{1c}}{\bar{T}_c}\right) + \frac{\bar{U}_c''}{\bar{U}_c'}\left(\frac{\bar{U}_{1c}'}{\bar{U}_c'} - \frac{\bar{U}_{1c}''}{\bar{U}_c''}\right) - \frac{2\alpha^2}{\bar{\alpha}^2}\left(\frac{\bar{T}_c'}{\bar{T}_c} - \frac{\bar{U}_c''}{\bar{U}_c'} + \frac{1}{r_c}\right)\frac{\bar{U}_{1c}}{\bar{U}_c}. \end{aligned}\right\} \tag{5.10}$$

Multiplying the inhomogeneous Rayleigh equation by $r\bar{T}\hat{p}_0/(\bar{U}-c)^2$ and integrating by parts, we arrive at the solvability condition

$$-\frac{r_c}{\bar{U}_c'}\left\{3(c^+ - c^-) - \frac{2\bar{\alpha}^2}{\bar{T}_c}\left[\frac{\mathrm{i}}{\alpha}\left(\frac{\partial A}{\partial \bar{t}} + c\frac{\partial A}{\partial \bar{x}}\right) - \bar{U}_{1c}\bar{x}A\right]\left(\frac{\bar{T}_c'}{\bar{T}_c} - \frac{\bar{U}_c''}{\bar{U}_c'} + \frac{1}{r_c}\right)(a^+ - a^-)\right.$$
$$\left. - \bar{\alpha}^2 d(a^+ - a^-)\right\} = \frac{2\mathrm{i}}{\alpha}\left[cI_2\frac{\partial A}{\partial \bar{x}} + I_3\frac{\partial A}{\partial \bar{t}}\right] - (\bar{x}A)I_1 \tag{5.11}$$

where

$$I_1 = \int_0^\infty \left\{ \left[\frac{2\bar{U}'}{\bar{U}-c}\left(\frac{\bar{U}_1}{\bar{U}-c} - \frac{\bar{U}_1'}{\bar{U}'}\right) + \frac{T'}{T}\left(\frac{\bar{T}_1'}{\bar{T}'} - \frac{\bar{T}_1}{\bar{T}}\right)\right] \frac{\bar{T}(r\hat{p}_0\hat{p}_0')}{(\bar{U}-c)^2} + \alpha^2 M^2 \left(\frac{2\bar{U}_1}{\bar{U}-c} - \frac{\bar{T}_1}{\bar{T}}\right) r\hat{p}_0^2 \right\} \mathrm{d}r,$$

$$I_2 = \int_0^\infty \left\{ \frac{\bar{T}\bar{U}'(r\hat{p}_0\hat{p}_0')}{(\bar{U}-c)^4} + \frac{\alpha^2}{c}\left[\frac{M^2\bar{U}}{(\bar{U}-c)} - \frac{\bar{T}}{(\bar{U}-c)^2}\right] r\hat{p}_0^2 \right\} \mathrm{d}r,$$

$$I_3 = \int_{-\infty}^\infty \left\{ \frac{\bar{T}\bar{U}'(r\hat{p}_0\hat{p}_0')}{(\bar{U}-c)^4} + \frac{\alpha^2 M^2 r\hat{p}_0^2}{\bar{U}-c} \right\} \mathrm{d}r.$$

The jumps $(a^+ - a^-)$ and $(c^+ - c^-)$ will be calculated in § 5.3 by considering the flow within the critical layer.

5.2. *Mach wave field*

It can be shown that $\hat{p}_1 \sim O(r^{1/2})$ for $r \gg 1$. Therefore the main-layer expansion (5.2) breaks down when $r \sim R^{1/2}$, and the large-r asymptote of the instability mode (5.5) cannot fully represent the radiated Mach wave field. Analogous to the planar case, the Mach wave field consists of two regions. The near field corresponds to $r \sim R^{1/2}$, and thus we introduce

$$\bar{r} = R^{-1/2} r = O(1). \tag{5.12}$$

The pressure expands as

$$p = \epsilon R^{-1/4}\left(p_0 + R^{-1/2} p_1 + \cdots\right), \tag{5.13}$$

and similar expansions hold for other quantities. As is expected, the leading-order term p_0 is governed by the standard acoustic equation

$$M_a^2 \frac{\partial^2 p_0}{\partial t^2} - \left(\frac{\partial^2}{\partial r^2} + \frac{1}{r}\frac{\partial}{\partial r} + \frac{\partial^2}{\partial x^2}\right) p_0 = 0, \tag{5.14}$$

where $M_a = M/T_a^{1/2}$, i.e. the Mach number based on the ambient sound speed.

Note that the equation applies to helical as well as to axisymmetric disturbances. This is because the term corresponding to the azimuthal variation, m^2/r^2, diminishes in the acoustic region. The Mach wave therefore is quasi-axisymmetric. Equation (5.14) has the solution

$$p_0 = \bar{p}_0(\bar{x}, \bar{r}, \bar{t})\, \mathrm{e}^{\mathrm{i}\alpha(x+qr-ct)} \cos(m\theta) + \text{c.c.},$$

consistent with (5.5). As in the planar case, the envelope function $\bar{p}_0$ can be determined by considering p_1. The latter is found to satisfy the equation

$$M_a^2 \frac{\partial^2 p_1}{\partial t^2} - \left(\frac{\partial^2}{\partial r^2} + \frac{1}{r}\frac{\partial}{\partial r} + \frac{\partial^2}{\partial x^2}\right) p_1 = 2\frac{\partial^2 p_0}{\partial r \partial \bar{r}} + 2\frac{\partial^2 p_0}{\partial x \partial \bar{x}} + \frac{1}{\bar{r}}\frac{\partial p_0}{\partial r} - 2M_a^2 \frac{\partial^2 p_0}{\partial t \partial \bar{t}}.$$

To prevent a secular term in the solution for p_1 from occurring on the scale of $x = O(1)$, we require the right-hand side to vanish, and this leads to

$$2q\frac{\partial \bar{p}_0}{\partial \bar{r}} + 2\frac{\partial \bar{p}_0}{\partial \bar{x}} + \frac{q}{\bar{r}}\bar{p}_0 + 2M_a^2 c \frac{\partial \bar{p}_0}{\partial \bar{t}} = 0.$$

Moreover, matching with the main-deck solution (see (5.5)) requires

$$\bar{p}_0 \to \frac{\mathscr{C}_\infty}{\sqrt{\bar{r}}} A(\bar{x}, \bar{t}) \quad \text{as} \quad \bar{r} \to 0. \tag{5.15}$$

The appropriate solution is found to be

$$\bar{p}_0 = \frac{\mathscr{C}_\infty}{\sqrt{\bar{r}}} A(\bar{\xi}, \bar{\eta}), \quad \text{with} \quad \bar{\xi} = \bar{x} - \bar{r}/q, \quad \bar{\eta} = \bar{t} - \left(M_a^2 c/q\right)\bar{r}. \tag{5.16}$$

In summary, for both axisymmetric and helical supersonic instability modes, the instantaneous field of the radiated Mach wave is described by the formula

$$p_0 = \frac{\mathscr{C}_\infty}{\sqrt{\bar{r}}} A\left(\bar{x} - \bar{r}/q, \bar{t} - M_a^2 c/q\,\bar{r}\right) \mathrm{e}^{\mathrm{i}\alpha(x+qr-ct)} \cos(m\theta) + \text{c.c.} \tag{5.17}$$

The simple interpretation of the radiation process in terms of the characteristics, as given in § 4.1 for the planar case, still applies provided that $\sqrt{r}\,p_0$ is taken to represent the Mach wave field. Specifically, the acoustic energy flux $r|p_0|^2$ propagates along the characteristics $\bar{\xi} = \text{constant}$.

Suppose that $A(\bar{x})$ attains its maximum at $\bar{x}_s$. Then formula (5.16) represents a pattern of waves which appear to be radiated from a source at $\bar{x}_s$. This prediction is consistent with the experimental observation of Troutt & McLaughlin (1982). We note that the DNS results of Mitchell *et al.* (1997), as presented in their figure 4, clearly exhibit this feature. Further comparisons will be made in § 6.

The above analysis can be carried out to high orders. Consideration of p_1 shows that $p_1 \sim \sqrt{\bar{r}} A(\bar{x} - \bar{r}/q, \bar{t} - M_a^2 c/q\bar{r})$, which implies that expansion (5.13) breaks down when $\bar{r} \sim R^{1/2}$. As in the planar case, we now seek an appropriate solution in the far field of the Mach wave beam, corresponding to

$$\bar{r} = O\left(R^{1/2}\right), \quad \bar{\xi} = O(1), \tag{5.18}$$

by introducing the variable

$$\tilde{r} = R^{-1/2}\bar{r} = R^{-1} r. \tag{5.19}$$

The large-$\bar{r}$ asymptote of p_0 and p_1 suggests that the solution for the pressure should expand as

$$p = \epsilon R^{-1/2}[\tilde{p}_0(\bar{\xi}, \bar{\eta}, \tilde{r}) + R^{-1}\tilde{p}_1(\bar{\xi}, \bar{\eta}, \tilde{r}) + \cdots] \mathrm{e}^{\alpha(x+qr-ct)} \cos m\theta + \text{c.c.}$$

The secular condition for $\tilde{p}_1$ yields the equation governing $\tilde{p}_0$:

$$2\mathrm{i}\alpha q \frac{\partial \tilde{p}_0}{\partial \tilde{r}} + q^{-2} M_a^2 \left\{ c^2 \frac{\partial^2 \tilde{p}_0}{\partial \bar{\xi}^2} + 2c \frac{\partial^2 \tilde{p}_0}{\partial \bar{\xi}\,\partial \bar{\eta}} + \frac{\partial^2 \tilde{p}_0}{\partial \bar{\eta}^2} \right\} + \frac{\mathrm{i}q}{\tilde{r}} \tilde{p}_0 = 0. \tag{5.20}$$

In order to match (5.16), $\tilde{p}_0$ must satisfy

$$\tilde{p}_0 \to \frac{\mathscr{C}_\infty}{\sqrt{\tilde{r}}} A(\bar{\xi}, \bar{\eta}) \quad \text{as} \quad \tilde{r} \to 0. \tag{5.21}$$

In the case of a single wave, for which A is a function of $\bar{x}$ only, the solution to (5.20)–(5.21) is found to be

$$\tilde{p}_0(\bar{\xi}, \tilde{r}) = \frac{\mathrm{e}^{-\pi\mathrm{i}/4}}{\tilde{r}} \left(\frac{\alpha q^3}{2\pi M_a^2 c^2} \right)^{1/2} \mathscr{C}_\infty \int_{-\infty}^{\infty} A(\zeta) \exp\left\{ \frac{\mathrm{i}\alpha q^3}{2M_a^2 c^2 \tilde{r}} (\bar{\xi} - \zeta)^2 \right\} \mathrm{d}\zeta. \tag{5.22}$$

For the case of a modulated wavetrain, solving (5.20)–(5.21) by Fourier transform with respect to $\bar{\eta}$, we obtain

$$\widehat{P}(\bar{\xi}, \tilde{\omega}, \tilde{r}) = \frac{\mathrm{e}^{-\pi\mathrm{i}/4}}{\tilde{r}} \left(\frac{\alpha q^3}{2\pi M_a^2 c^2} \right)^{1/2} \mathscr{C}_\infty \widehat{Q}(\bar{\xi}, \tilde{\omega}, \tilde{r}) \exp\left\{ -\frac{\mathrm{i}M_a^2 \tilde{\omega}^2 \tilde{r}}{2\alpha q^3} \right\} \tag{5.23}$$

where $\widehat{P}$ denotes the Fourier transform of $\tilde{p}_0$, and

$$\widehat{Q}(\bar{\xi},\tilde{\omega},\tilde{r}) = \int_{-\infty}^{\infty} \widehat{A}(\zeta,\tilde{\omega}) \exp\left\{ \frac{\mathrm{i}\alpha q^3}{2M_a^2 c^2 \tilde{r}} \left(\bar{\xi} - \zeta + \frac{M_a^2 c\,\tilde{\omega}\tilde{r}}{\alpha q^3} \right)^2 \right\} \mathrm{d}\zeta. \tag{5.24}$$

For a wavepacket with a frequency bandwidth Δ^{-1}, the 'time averaged' acoustic intensity can be expressed as

$$\overline{(\tilde{p}_0)^2} = \frac{1}{\tilde{r}^2} \left(\frac{\alpha q^3 |\mathscr{C}_\infty|^2}{4\pi^2 M_a^2 c^2 \Delta} \right) \int_{-\infty}^{\infty} |\widehat{Q}(\xi,\tilde{\omega},\tilde{r})|^2 \,\mathrm{d}\tilde{\omega}. \tag{5.25}$$

The solution (5.16) for the Mach wave is valid for $\bar{r} = O(1)$, i.e. in the region $r \sim R^{-1/2} R_J$. From the asymptotic point of view, this could be a quite large region for high-Reynolds-number jets so that the near-field solution (5.16), which is attractive owing to its simplicity, may suffice for prediction purpose. However, translated to numerical values the validity region of (5.16) is found to be within just a few jet exit diameters in certain situations. The far-field solution (5.22) or (5.25) must be employed. Further elucidation of the relation between the near- and far-field solutions will be given in § 6, when specific flows are investigated.

As in planar flows, Mach waves in a circular jet also concentrate in the beam $\bar{\xi} = O(1)$, which has an intrinsic direction. In fact, the solution for a circular jet differs from that for a plane mixing layer or jet merely by a factor $1/\sqrt{\tilde{r}}$; this factor entirely takes account of the effect of cylindric geometry to the required order. Note that the solutions for the Mach waves radiated by axisymmetric and helical modes are formally the same. The difference, however, lies somewhat indirectly in the amplitude function A, which is governed by quite different evolution equations, as will be shown in the next subsection.

5.3. *Amplitude equation*

To derive the amplitude equation, one first has to calculate the jumps $(a^+ - a^-)$ and $(c^+ - c^-)$ by considering critical-layer dynamics. It is then necessary to consider the axisymmetric and helical modes separately, because nonlinearity operates differently.

5.3.1. *Axisymmetric supersonic mode*

For an axisymmetric supersonic mode ($m = 0$), the dominant nonlinear effect is associated with the singularity of simple-pole form in the temperature fluctuation as well as the logarithmic singularity in the velocity fluctuation. This is similar to the planar case, and so the same scaling applies: the mode evolves nonlinearly when (cf. (2.2))

$$\epsilon = R^{-11/12}. \tag{5.26}$$

The critical-layer expansion remains the same as (3.11), and the relevant analysis is by and large similar to that of the planar case. Specifically the solutions for Θ_1 and U_1 are given by (3.13) and (3.14) respectively except that $(\bar{T}_c'/\bar{T}_c - \bar{U}_c''/\bar{U}_c')$ in the latter is replaced by $(\bar{T}_c'/\bar{T}_c - \bar{U}_c''/\bar{U}_c' + 1/r_c)$. The remaining nonlinear interactions are virtually identical. We therefore omit the details, and present only the final results:

$$a^+ - a^- = -\widehat{k}\pi\mathrm{i}, \tag{5.27}$$

$$c^+ - c^- = -\frac{\bar{\alpha}^2}{3\bar{T}_c} \left[\frac{\mathrm{i}}{\alpha} \left(\frac{\partial A}{\partial \bar{t}} + c \frac{\partial A}{\partial \bar{x}} \right) - \bar{U}_{1c} \bar{x} A \right] j\pi\mathrm{i} - \frac{\bar{\alpha}^2 \bar{U}_c'}{3\bar{T}_c} \bar{x} A j_1 \pi\mathrm{i} - \frac{\bar{\alpha}^2}{3} \widehat{k} d\pi\mathrm{i} - \frac{\Lambda}{3} A|A|^2, \tag{5.28}$$

where Λ is a slightly modified version of the planar case (cf. (3.25)):

$$\Lambda = \frac{\pi\alpha^4\bar{U}_c'^2}{3\bar{T}_c^2\mu_c}\left\{\frac{\bar{T}_c'(\bar{T}_c\mu_c' - \kappa_c)}{\bar{T}_c(\mu_c - \kappa_c)}\left(\left(\frac{\mu_c}{\kappa_c}\right)^{4/3} - 1\right) + \widehat{k} + \frac{\bar{T}_c'}{\bar{T}_c}\left(1 + \frac{\mu_c}{\kappa_c}\right)^{2/3}\left(\frac{2\mu_c}{\kappa_c}\right)^{1/3}\right\}(2s)^{-1/3}\Gamma\left(\tfrac{1}{3}\right). \tag{5.29}$$

In the present axisymmetric case, $\bar{\alpha} = \alpha$ and $\widehat{k} = (\bar{T}_c'/\bar{T}_c - \bar{U}_c''/\bar{U}_c' + 1/r_c)$. Inserting (5.27)–(5.28) into the solvability condition (5.11), we obtain the same form of amplitude equation as in the planar case:

$$\frac{\partial A}{\partial \bar{x}} + c_g^{-1}\frac{\partial A}{\partial \bar{t}} = \sigma\bar{x}A + lA|A|^2, \tag{5.30}$$

but the expressions for the coefficients are modified, namely

$$c_g = cG\Big/\left\{2I_3 - \frac{\bar{\alpha}^2 r_c}{\bar{T}_c\bar{U}_c'}\left[j - 2\left(\frac{\bar{T}_c'}{\bar{T}_c} - \frac{\bar{U}_c''}{\bar{U}_c'} + \frac{1}{r_c}\right)\widehat{k}\right]\pi\mathrm{i}\right\}, \tag{5.31}$$

$$\sigma = (-\mathrm{i}\alpha/c)\left\{I_1 - \frac{\bar{\alpha}^2 r_c}{\bar{T}_c}\left[\frac{\bar{U}_{1c}}{\bar{U}_c'}\left(j - 2\left(\frac{\bar{T}_c'}{\bar{T}_c} - \frac{\bar{U}_c''}{\bar{U}_c'} + \frac{1}{r_c}\right)\widehat{k}\right) - j_1\right]\pi\mathrm{i}\right\}\Big/G, \tag{5.32}$$

$$l = -\mathrm{i}\alpha\, r_c\Lambda/(c\bar{U}_c'G), \tag{5.33}$$

where

$$G = 2I_2 - \frac{\bar{\alpha}^2 r_c}{\bar{T}_c\bar{U}_c'}\left[j - 2\left(\frac{\bar{T}_c'}{\bar{T}_c} - \frac{\bar{U}_c''}{\bar{U}_c'} + \frac{1}{r_c}\right)\widehat{k}\right]\pi\mathrm{i}.$$

5.3.2. *Pairs of helical modes*

As was pointed out by Wu *et al.* (1993), the leading-order nonlinear interaction between a pair of helical modes in a circular jet is similar to an oblique pair in a planar shear flow, the reason being that the critical layer is very thin so that the azimuthal curvature becomes negligible. The dominant nonlinear effect is now associated with the singularity of a simple-pole form in the outer solution for the streamwise and spanwise velocities (see (5.8)), while that associated with compressibility and the logarithmic singularity becomes secondary. If the amplitude of the instability mode $\epsilon \sim R^{-1}$ (or larger), the critical-layer dynamics would be non-equilibrium and evolve over the length scale of $O(R^{1/3})$ (or shorter). Again the Mach wave radiation of such rapidly evolving modes is left for future study; see also § 7.

For the present regime of interest over an $O(R^{1/3})$ length scale, the helical modes evolve nonlinearly on the scale $\bar{x} = O(1)$ at the threshold order of magnitude

$$\epsilon = R^{-7/6}, \tag{5.34}$$

which is much smaller than that for an axisymmetric modes (cf. (5.26)). The typical numerical size of the amplitude corresponding to (5.34) will be estimateed in § 6.

For the present interacting helical modes, the jumps are as given by (5.27)–(5.28), but the nonlinear term in (5.28) is now replaced by

$$-\frac{\Lambda}{3}A\int_0^\infty |A(\bar{x} - \xi, \bar{t} - \xi/c)|^2\,\mathrm{d}\xi$$

with

$$\Lambda = \frac{\pi}{c}\alpha^{-5/3}\bar{U}_c'|\bar{U}_c'|^{1/3}(\bar{T}_c\mu_c)^{-4/3}\left(\tfrac{2}{3}\right)^{2/3}\Gamma\left(\tfrac{1}{3}\right)\left(\alpha^2 - \frac{m^2}{r_c^2}\right)\frac{m^4}{r_c^4}. \tag{5.35}$$

This nonlinear term is the highly viscous limit of the nonlinear term given in Wu *et al.* (1993) and Lee & Leib (1995); in making this identification m/r_c plays the role of a

spanwise wavenumber. Use of these jumps in the solvability condition (5.11) yields the amplitude equation

$$\frac{\partial A}{\partial \bar{x}} + c_g^{-1}\frac{\partial A}{\partial \bar{t}} = \sigma \bar{x} A + lA\int_0^\infty |A(\bar{x}-\xi, \bar{t}-\xi/c)|^2\,\mathrm{d}\xi, \tag{5.36}$$

where the coefficients c_g^{-1}, σ and l are given by (5.31), (5.32) and (5.33) respectively. Equation (5.36) must be solved numerically. For a modulated wavepacket, for the convenience of calculating the radiated Mach wave, (5.36) is solved in the spectral space, and so it is Fourier transformed to

$$\widehat{A}'(\bar{x}, \tilde{\omega}) = \left(\sigma \bar{x} - \mathrm{i}c_g^{-1}\tilde{\omega}\right)\widehat{A} + \frac{l}{(2\pi)^2}\int_{-\infty}^{\infty}\int_{-\infty}^{\infty}\widehat{A}(\bar{x}, \tilde{\omega}-\tilde{\omega}_1)\widehat{D}(\bar{x}, \tilde{\omega}_1, \tilde{\omega}_2)\,\mathrm{d}\tilde{\omega}_2\,\mathrm{d}\tilde{\omega}_1, \tag{5.37}$$

with

$$\widehat{D}(\bar{x}, \tilde{\omega}_1, \tilde{\omega}_2) = \int_0^\infty \widehat{A}(\bar{x}-\xi, \tilde{\omega}_2)\widehat{A}^*(\bar{x}-\xi, \tilde{\omega}_2-\tilde{\omega}_1)\,\mathrm{e}^{-(\mathrm{i}\tilde{\omega}_1/c)\xi}\,\mathrm{d}\xi. \tag{5.38}$$

Equation (5.37) is to be solved subject to the initial condition

$$\widehat{A}(\bar{x}, \tilde{\omega}) \to a_s(\tilde{\omega})\exp\left(\tfrac{1}{2}\sigma\bar{x}^2 - \mathrm{i}c_g^{-1}\tilde{\omega}\bar{x}\right) \quad \text{as} \quad \bar{x} \to -\infty. \tag{5.39}$$

6. Parametric study and comparisons with DNS and experiments

6.1. *The base flow*

In the numerical computation, the mean velocity profile is taken to be (Tam & Burton 1984*a*, *b*)

$$\bar{U} = \begin{cases} 1, & r \leqslant h \\ \exp\left\{-\left(\dfrac{r-h}{b}\right)^2\right\}. & r > h. \end{cases} \tag{6.1}$$

For simplicity the Prandtl number is assumed to be unity so that the temperature profile is given by Crocco's relation

$$\bar{T} = \left(1 + \frac{\gamma-1}{2}M^2\right)[T_a + (1-T_a)\bar{U}] - \frac{\gamma-1}{2}M^2\bar{U}^2, \tag{6.2}$$

where h and b characterize the centre and width of the shear layer respectively, and both of them are functions of x_3. The conservation of momentum means that

$$\int_0^\infty \bar{R}\bar{U}^2 r\,\mathrm{d}r = 1/2,$$

which, on substituting in $\bar{U}$ and $\bar{R} = 1/\bar{T}$, imposes the relation

$$h^2 + 2J_0 bh + (2J_1 b^2 - 1) = 0 \tag{6.3}$$

between h and b, where

$$J_k = \int_0^\infty \zeta^k\,\mathrm{e}^{-2\zeta^2}\left[\left(1+\frac{\gamma-1}{2}M^2\right)\left(T_a + (1-T_a)\,\mathrm{e}^{-\zeta^2}\right) - \frac{\gamma-1}{2}M^2\,\mathrm{e}^{-2\zeta^2}\right]^{-1}\mathrm{d}\zeta \quad (k=0,\ 1).$$

For a properly chosen h or b, formula (6.1) is able to describe the development of the streamwise velocity profile from the nozzle exit to the fully developed region (Tam & Burton 1984*a*, *b*). A global function relation, however, is not needed for the present

study, since the focus is on the $O(R^{-1/2})$ vicinity of the neutral position $x_{3,n}$. Close to $x_{3,n}$, it suffices to express $b(x_3)$ as a Taylor series:

$$b(x_3) = b_n + \sigma_s(x_3 - x_{3,n}) + O((x_3 - x_{3,n})^2) \approx b_n + \sigma_s R^{-1/2}\bar{x},$$

where σ_s is the familiar spreading rate of the jet. It follows from differentiating (6.3) and (6.1) that

$$\frac{\mathrm{d}h}{\mathrm{d}x_3} = -\frac{1}{h + J_0 b_n}(2J_1 b + J_0 h)\sigma_s,$$

$$\bar{U}_1 = \begin{cases} 0, & r \leqslant h \\ 2\sigma_s\left[\dfrac{(r-h)^2}{b_n^3} - \dfrac{r-h}{b_n^2(h + J_0 b)}(2J_1 b_n + J_0 h)\right]\exp\left\{-\left(\dfrac{r-h}{b_n}\right)^2\right\}, & r > h. \end{cases}$$

The value of b_n determines the frequency of the local neutral instability mode, and vice versa (that is, a linearly neutral mode of a given frequency can be found only for a particular b_n).

6.2. *Characteristics of the eigenmodes and Mach wave front*

The compressible Rayleigh equation (5.3) is solved by employing a shooting method based on a fourth-order Runge–Kutta integrator. For an initial guess for the wavenumber α and phase speed c, (5.4) and (5.5) are used to integrate (5.3) from $r = r_0(=0.01)$ and $r = r_\infty(\approx 20)$ respectively to the positions just beneath and above the critical level, $(r_c - d)$ and $(r_c + d)$ say, where d is taken to be small, typically $d = 0.025$ and 0.05. The values of $\hat{p}_0$ at these two locations are equated to those given by the asymptotic solution (5.6), from which we can extract $a_\pm$. The normalization, $\hat{p}_0(r_c) = \bar{U}_c'/\bar{T}_c$ as implied by (5.6), also fixes the constants $\mathscr{C}_0$ and $\mathscr{C}_\infty$. The jump condition (5.27) is then used to update α and c until a preset tolerance is met.

Once the eigenvalue and eigenfunction are obtained, the coefficients in the amplitude equations can be evaluated. The Hadamard finite parts of the integrals involved are treated as follows. By using the relevant asymptotic solutions at r_c and ∞, the singular parts of the integrands are subtracted out so that the resulting integrands are regular. These are then evaluated numerically using Simpson's rule, whilst the singular parts are dealt with analytically.

The parameters are chosen guided primarily by the experiments of Troutt & McLaughlin (1982). In all the calculations, we take $T_a = 1$, and $M = 2.1$ unless otherwise stated. For the convenience of comparing with experiments, we introduce the Strouhal number $St = 2R_J f^*/U_J$, which is related to the frequency $\omega = \alpha c$ by $St = \omega/\pi$, where f^* is the physical frequency in units of Hertz.

Figures 2(*a*) and 2(*b*) show the eigenfunctions of the axisymmetric and helical supersonic modes respectively. Evidently these modes are radiative in character. It is interesting to note that the eigenfunctions quickly approach the asymptote (5.5) within a radial distance of just one to two diameters of the jet nozzle. The unsteady fluctuation in the majority of the flow field is therefore acoustic in nature.

Figures 3(*a*) and 3(*b*) show the wavenumbers and phase speeds of neutral modes for a range of frequencies. Also shown are the experimental data of Troutt & McLaughlin (1982). These agree remarkably well with the theoretical results for helical modes, but appear to differ from those for the axisymmetric modes. In particular, the phase speed of the axisymmetric modes behaves quite differently: it decreases with St rather than increases as for helical modes. This suggests that the helical modes are

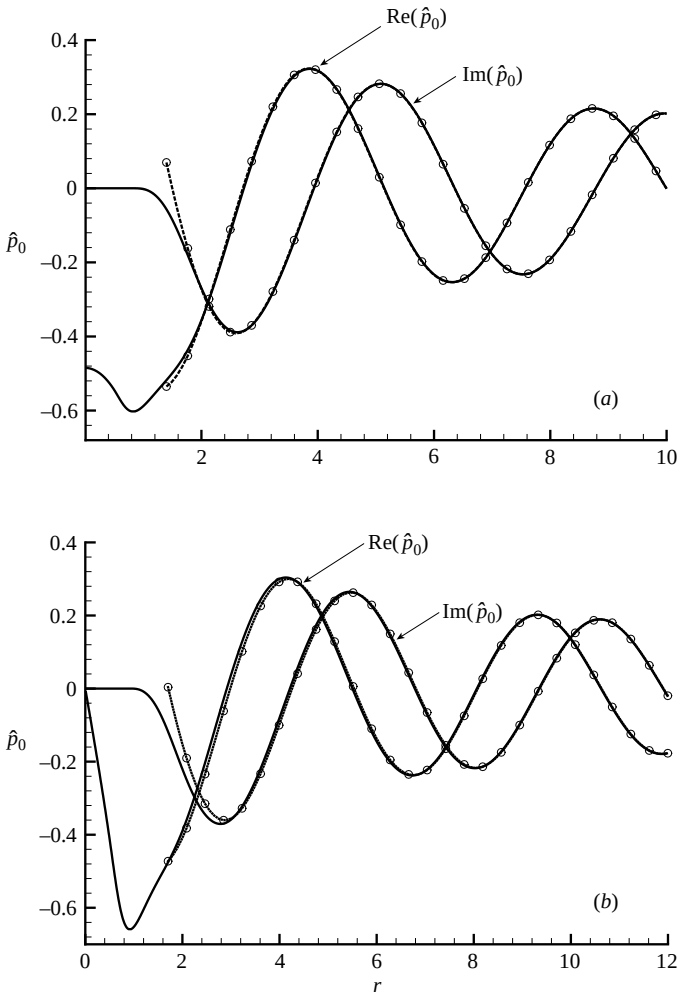

FIGURE 2. Eigenfunctions of supersonic instability modes in a $M = 2.1$ jet: (*a*) symmetric mode with $St = 0.4$, and (*b*) helical modes ($m = \pm 1$) with $St = 0.4$. The far-field asymptote (5.5) is represented by $\cdots\bigcirc\cdots$.

the predominated disturbances in the experiments. It should be mentioned that as an instability mode of a given St evolves downstream, its wavelength and phase speed change, and so strictly speaking the measured data may depend on streamwise locations. But measurements were usually carried out within a few diameters from the jet nozzle, within which the wavelength and speed do not vary significantly so that the comparison is meaningful. Troutt & McLaughlin (1982) found that the measured wavenumbers agreed well with the calculations using a vortex sheet model (Tam 1972). Further comparisons of this kind were presented by Tam & Hu (1989). Presumably, the wavenumbers are not particularly sensitive to the choice of the base-flow profiles. A notable feature of the phase speed is that it remains almost constant for all modes with $St > 0.3$.

The eigenvalue of the Rayleigh equation yields information on Mach wave phase fronts, which correspond to $x + qr - ct = \text{constant}$. Thus at any instant, the Mach

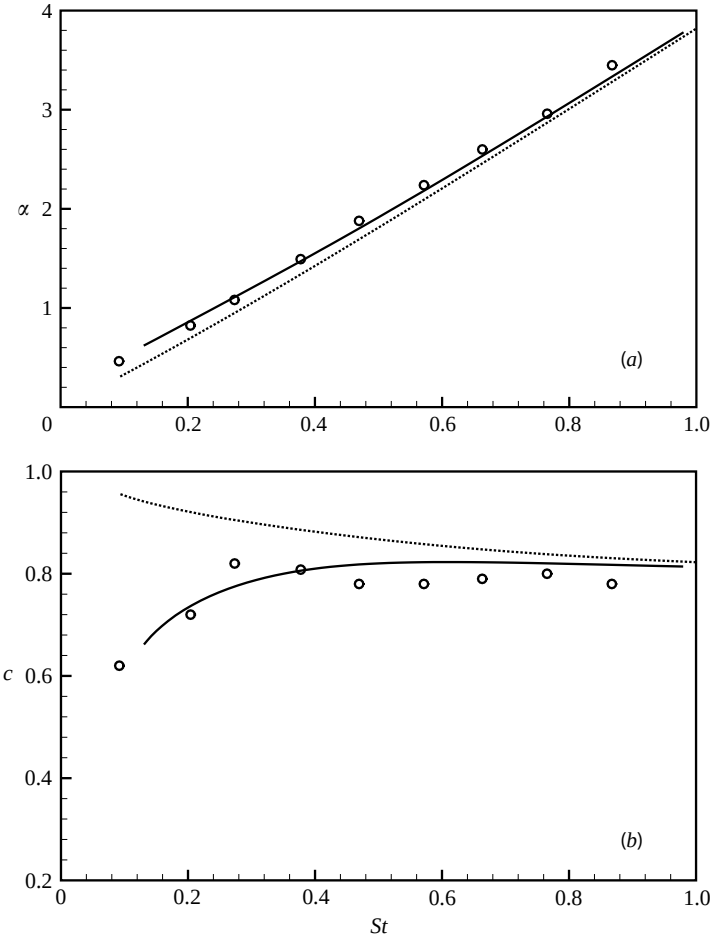

FIGURE 3. (*a*) Wavenumber α, and (*b*) phase speed c of neutral modes vs. frequency St. Theory results: ——, helical modes; · · · · · ·, axisymmetric modes. Experimental data (Troutt & McLaughlin 1982): ○.

wave fronts are parallel lines that make angle

$$\psi = \sin^{-1}\frac{1}{1+q^2} = \sin^{-1}\frac{1}{M_a c}$$

with the upstream axial direction. This result is consistent with the wavy-wall analogy for Mach wave emission. The prediction for ψ is displayed in figure 4 for both helical and axisymmetric modes at $M = 2.1$. The observed $\psi \approx 56^\circ$ for $St = 0.4$ in the experiments of Troutt & McLaughlin (1982) agrees with the theory, confirming that the acoustic field is primarily in the form of a Mach wave. Curiously, for $St = 0.2$, Troutt & McLaughlin found $\psi = 48^\circ$, which is considerably smaller than the theoretically expected value; the reason for this rather puzzling discrepancy remains unknown. The earlier experiments of McLaughlin *et al.* (1975), which were conducted at a somewhat lower Reynolds number, reported that $\psi \approx 60^\circ$ for $St = 0.18$ and $M = 2.2$. This value is in excellent agreement with the prediction.

Figure 4 reveals an important feature: for all modes ($St > 0.3$), the angle ψ remains almost constant. This is a result of the phase speed c having a weak dependence

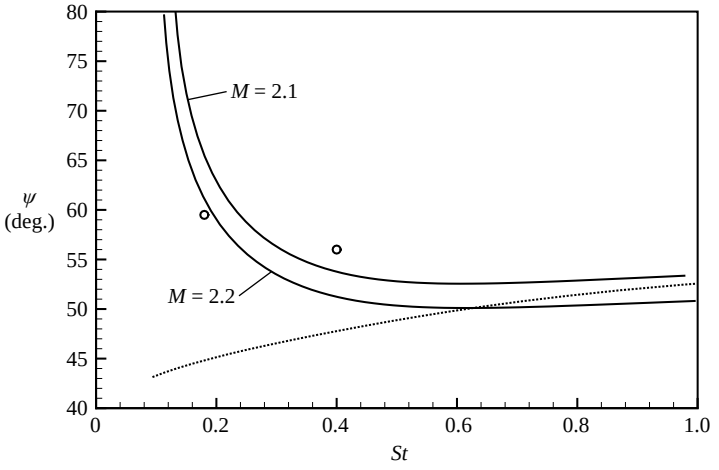

FIGURE 4. Mach angle ψ vs. frequency St. Theory results: ——, helical modes; ·····, axisymmetric modes. Experimental data (Troutt & McLaughlin 1982; McLaughlin *et al.* 1975): ○.

on St as shown in figure 3(b). Therefore, ψ is practically determined by just one parameter M_a, the jet Mach number based on the sound speed in the ambient fluid. Since these relatively high-frequency modes tend to be predominately present in the region close to the nozzle, and attenuate before the jet becomes fully developed, the upstream region of a jet would exhibit a characteristic Mach wave field which is highly organized even if it is generated by broadband instability waves. This conclusion is in agreement with observations (e.g. Lowson & Ollerhead 1968; Oertel 1979). The calculation of Tam & Hu (1989) indicates that the characteristic Mach wave angle can be predicted by a vortex sheet model for a wide range of Mach numbers.

6.3. *Directivity of Mach wave field*

The directivity of the Mach wave field is characterized by the solutions for the Mach wave envelope, as given by (5.16) in the near field and by (5.22) or (5.25) in the far field of the beam. These formulae are expressed in terms of $\bar{x}$, $\bar{r}$ and $\tilde{r}$. To order to facilitate direct comparison with experiments, they will be reverted back to x and r via (2.1), (5.12) and (5.19), the first of which can be more conveniently rewritten as

$$\bar{x} = R^{-1/2}(x - x_n), \tag{6.4}$$

where $x_n = x_n^*/R_J$, the neutral position x_n^* normalized by R_J.

First, we check (5.16) for the case of a simple axisymmetric instability mode against the DNS result of Mitchell *et al.* (1997). From the given parameters, it can be inferred that $\alpha = 1.51$, $c = 0.75$, $M = 4.47$ and $q = 1.12$. The instability wave in the simulation has a very small amplitude so that as it evolves through the neutral position its envelope is Gaussian, $A = a_0 \exp\{\sigma \bar{x}^2/2\} = a_0 \exp\{R^{-1}\sigma(x - x_n)^2/2\}$. Lacking detailed information about the mean flow, we are unable to calculate σ and x_n. Instead, we simply extrapolate σ and x_n by fitting $A \sim \exp\{R^{-1}\sigma(x - x_n)^2/2\}$ to the shape of the curve in their figure 3(a). By this practice, we isolate possible uncertainty or error in predicting the amplitude evolution from that associated with the formula (5.16) itself. Using this Gaussian envelope in (5.16) then yields the solution for the Mach wave envelope. The contours of $|\bar{p}_0|$ predicted by (5.16) are shown in figure 5, and they are to be compared with figure 4(a) in Mitchell *et al.* (1997). A close resemblance is evident. In the present case, the near-field solution is apparently

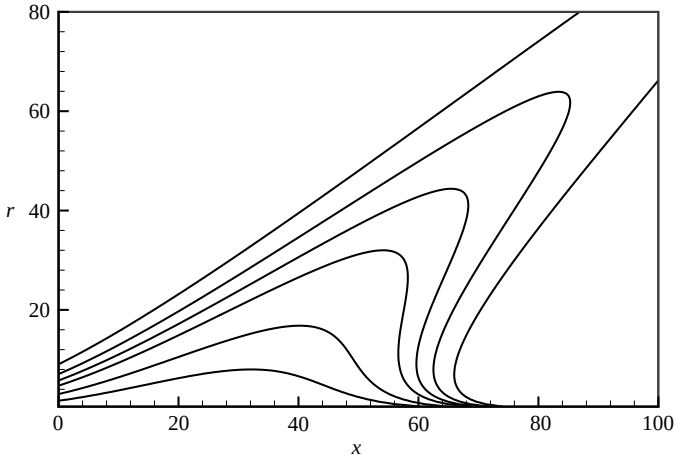

FIGURE 5. Contours of the pressure $|\bar{p}_0|$ as predicted by (5.16) using σ and x_n extracted by fitting a Gaussian envelope to the amplitude in figure 4(*a*) of Mitchell *et al.* (1997).

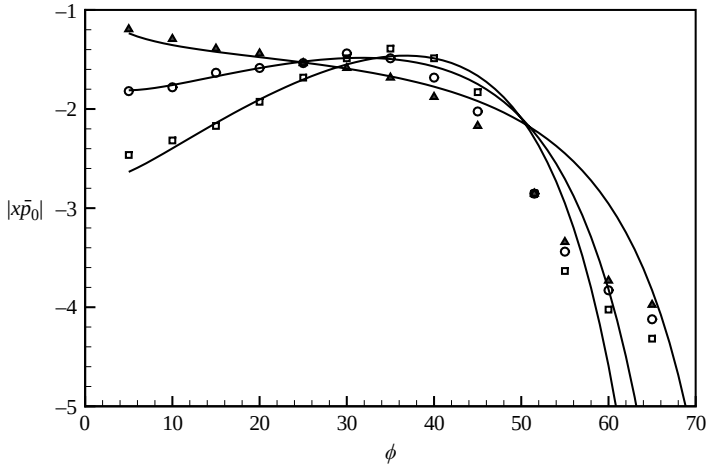

FIGURE 6. Directivity of the Mach wave field: $x|\bar{p}_0|$ vs. $\phi = \tan^{-1}(r/x)$ at different streamwise locations. Theoretical results are presented by solid lines, and the DNS results of Mitchell *et al.* (1997) by symbols: △, $x = 40$; ○, $x = 70$; ◇, $x = 90$.

valid in the region extending to $r = 80$. A close quantitative comparison is presented in figure 6, where $|x\bar{p}_0|$ is plotted (on a logarithmic scale) against $\phi = \tan^{-1}(r/x)$ at three different downstream locations. Here the initial amplitude a_0 is a free parameter, and is chosen such that $|x\bar{p}_0|$ equals the DNS value at $\phi = 38^\circ$, $x = 90$. The agreement is reasonably good. In particular, the acoustic intensity within the Mach wave beam is predicted well. The accuracy of (5.16) appears to deteriorate at large ϕ, which is not surprising because the near-field solution breaks down far away from the beam. It is emphasized that in this comparison only one value of a_0 is used.

We now present results for the profile (6.1), which models quite well the base flow in the experiments of Troutt & McLaughlin (1982). Attention will be focused on the

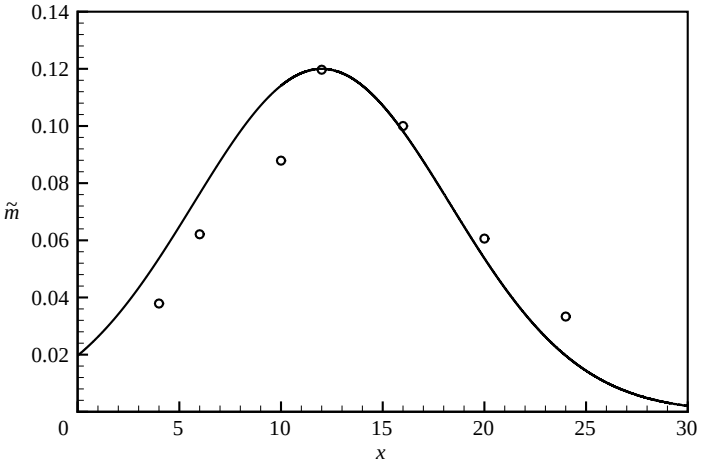

FIGURE 7. Amplitude of mass-velocity fluctuation $\tilde{m}$ vs. x for $St = 0.2$ and $M = 2.1$. Present theory: ——. Experiment (Troutt & McLaughlin 1982): ○.

modes with $St = 0.2$ and 0.4, which were the modes excited in a controlled manner. For a given St, by solving Rayleigh equation, we determine b_n for which this mode is neutral. Our b_n then is converted to the δ in Troutt & McLaughlin (1982) using the relation $\delta/R_J = \sqrt{2.773}b_n$. Using the experimental data in their figure 19, we can find the corresponding neutral location x_n and σ_s, which are used in (6.4) to allow a direct comparison between the theory and experiments.

The first calculation was performed for a helical mode with $St = 0.2$. Eigenvalue calculation shows that this mode is neutral for $b_n = 1.05$, which corresponds to $x_n \approx 12$ and $\sigma_s \approx 0.162R$. It then follows that $A = a_0 \exp\{R^{-1}\sigma(x-12)^2/2\}$, assuming a_0 to be sufficiently small. Note that σ is calculated from the theory rather than being extracted from the experimental data. The initial amplitude a_0 has to be chosen however. To that end, we consider the root-mean-square of the mass-velocity fluctuation, $\tilde{m} \equiv (\rho u)_{rms}$. By using the solutions for the velocity and density in the critical layer, it is found that

$$\tilde{m} = \sqrt{2}\frac{\alpha \bar{U}_c}{\bar{T}_c}\left(\frac{\bar{T}_c'}{\bar{T}_c} - \frac{m^2}{\alpha^2 r_c^2}\frac{\bar{U}_c'}{\bar{U}_c}\right) R^{-5/6}|A| \left| \int_0^\infty \exp\left(-s\xi^3 - \mathrm{i}\alpha \bar{U}_c' R^{-1/3}(r - r_c)\xi\right) \mathrm{d}\xi \right|. \tag{6.5}$$

In their experiments, Troutt & McLaughlin (1982) measured $\tilde{m}$ along the nozzle lip line, which at $x = 12$ happens to correspond to the R for which $\tilde{m}$ attains its maximum. We choose a_0 so that the calculated $\tilde{m}$ matches the measured value at $x = 12$. The prediction by (6.5) is plotted in figure 7 along with the experimental data. The overall agreement between the two is fair, indicating that the Gaussian envelope is able to capture the non-parallel effect that underlies the amplification and decaying process.

The Mach wave in the near field, as predicted by (5.16), is shown in figure 8(a). These pressure contours broadly capture the highly directional feature of Mach wave emission. However, the narrow, wedge-shaped contours are somewhat different from the lobed ones observed in experiments. In figure 8(b), the contours corresponding to the far-field solution (5.22) are plotted. Now the contours appear to be lobed. Several of these contours are also shown as dotted lines in figure 8(a) in order to see the relevance of the near- and far-field solutions. The comparison indicates that the near-field solution is applicable only in a region within just two diameters from the jet centre, where these two solutions overlap as expected. There arises the question as

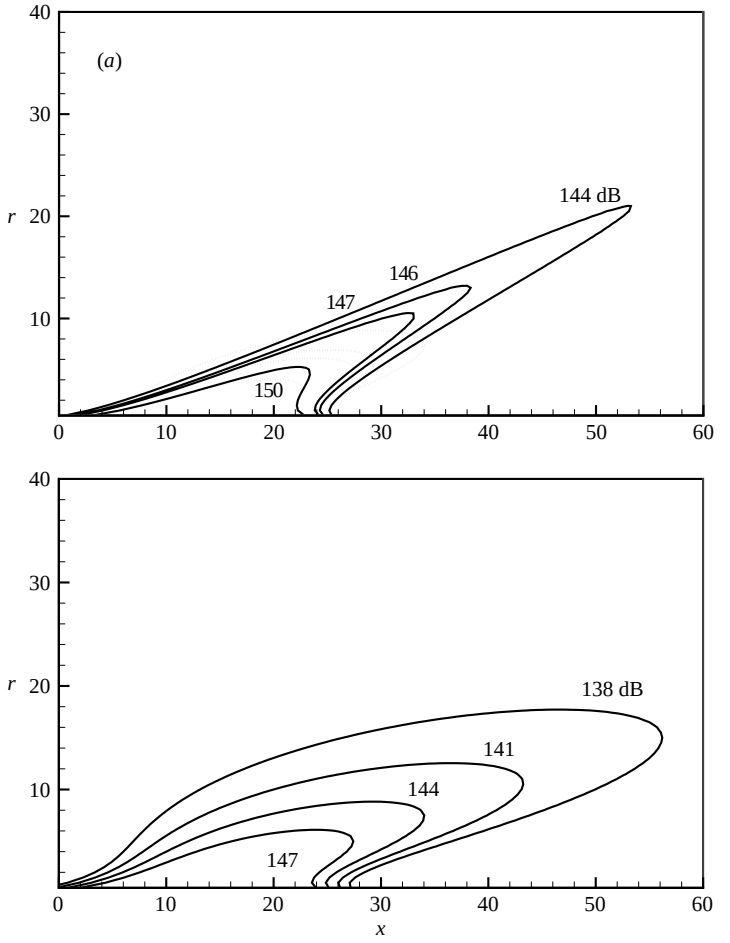

FIGURE 8. Pressure contours ($St = 0.2$): (a) as predicted by (5.16) (——) and (5.22) (· · · · · ·), and (b) in the far field.

to why the near-field solution has such a limited validity in the present case whilst a much extended validity was observed in the case shown in figure 5. This question can be answered by examining (5.22) for a linearly evolving instability wave, for which $A(\bar{x}) = \exp\{\sigma\bar{x}^2/2\}$. Then (5.22) simplifies to

$$\tilde{p}_0 = \frac{1}{\sqrt{\tilde{r}}}\left[1 - \left(\frac{\mathrm{i}M_a^2c^2\sigma}{\alpha q^3 R}\right)r\right]^{-1/2} \exp\left\{\tfrac{1}{2}\sigma\xi^2 \Big/ \left[1 - \left(\frac{\mathrm{i}M_a^2c^2\sigma}{\alpha q^3 R}\right)r\right]\right\}, \tag{6.6}$$

which reduces to the near-field solution

$$\bar{p}_0 = \frac{1}{\sqrt{\bar{r}}} \exp\left\{\tfrac{1}{2}\sigma\bar{\xi}^2\right\}$$

in the limit $M_a^2c^2\sigma/(\alpha q^3 R)r \ll 1$. Obviously, the size of the validity region of the near-field solution is determined by the parameter $M_a^2c^2\sigma/(\alpha q^3 R)$: the larger this parameter is, the smaller the validity region of the near-field solution becomes. In the present case, $M_a^2c^2\sigma/(\alpha q^3 R) = 0.518$ while in figure 5 it has a much smaller value of 0.013.

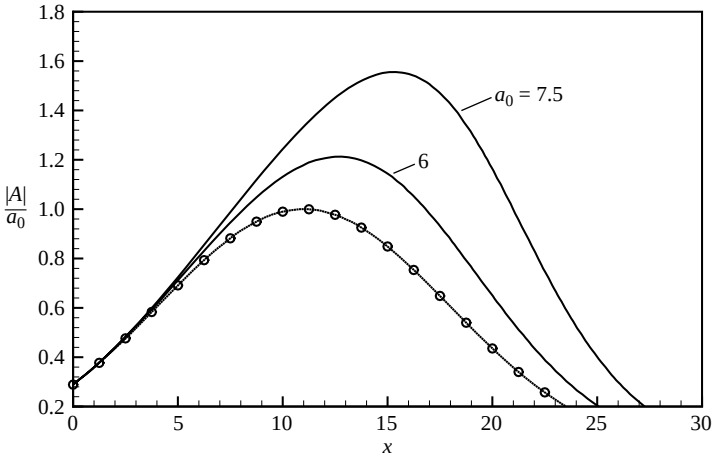

FIGURE 9. $|A/a_0|$ vs. x illustrating the nonlinear development of the axisymmetric mode with $St = 0.4$ with initial amplitudes $a_0 = 6$, 7.5. —○—, linear approximation.

The result (6.6) indicates that as r increases, the characteristic width of the Mach wave beam increases by the factor

$$\left|1 - \left(\frac{\mathrm{i}M_a^2 c^2 \sigma}{\alpha q^3 R}\right) r\right|^{1/2} > 1,$$

and on the other hand the overall intensity is reduced by the same factor. These two effects are clearly reflected in figure 8(b). While the contours shown in figure 8(b) are broadly similar to those in figure 29(a) of Troutt & McLaughlin (1982), there is an appreciable difference in detail: the beam predicted by the theory makes a smaller angle to the downstream axial direction than that observed in experiments. The absolute sound level is underestimated. Such discrepancies are not unexpected, because the sound level measured in the experiment, though band-passed, is still broadband in nature, consisting of contributions of all disturbances in the frequency range $St = 0.15$–0.23. Indeed the directivity and intensity of the overall sound pressure, shown in figure 27 of Troutt & McLaughlin (1982), differ quite appreciably from those of the band-passed pressure, indicating that spectral contents do make a difference. Tam & Burton (1984a, b) found that the observed contour pattern could be reproduced in their theory after an axisymmetric mode of suitable amplitude was included. However, without the information about the relative phase relation between the axisymmetric and helical modes, a completely convincing comparison is impossible.

We now consider the Mach waves radiated by instability waves which are undergoing nonlinear evolution. The first case is for an axisymmetric mode with $St = 0.4$, for which the Landau coefficient l in the amplitude equation (5.30) has a positive real part, i.e. nonlinearity has a destabilizing effect. Figure 9 displays several solutions for different initial amplitude a_0. Nonlinearity starts to have appreciable effect for $a_0 > 5$. By using the critical-layer solution for the density perturbation, it may be estimated that this corresponds to 3% peak density fluctuation, or 2.5% peak mass-flux fluctuation (as approximated by (6.5)). The fluctuations in the experiments of Troutt & McLaughlin (1982) are somewhat above this level, and so it seemed possible

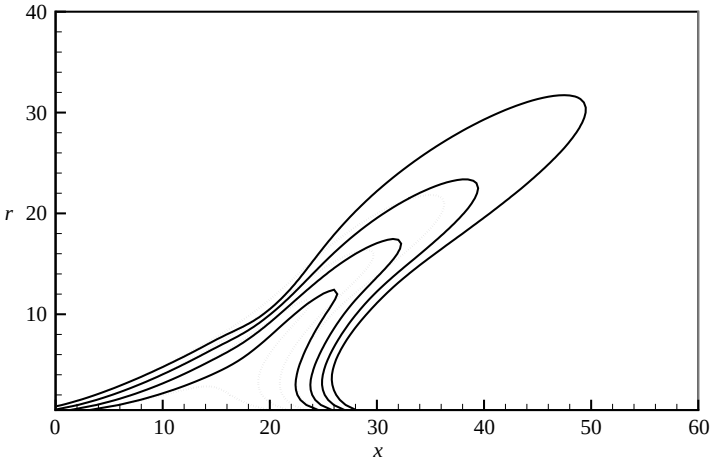

FIGURE 10. Pressure contours of Mach waves radiated by the axisymmetric mode with $St = 0.4$, predicted by (5.22) using the nonlinear solution (——) and linear approximation (· · · · · ·) for A.

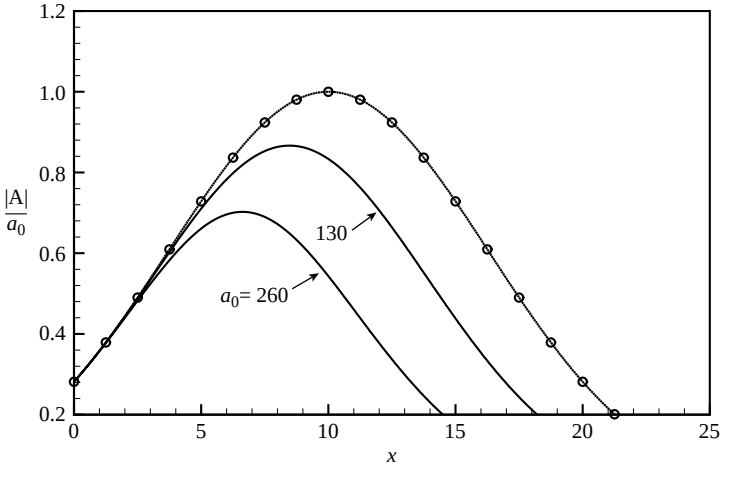

FIGURE 11. $|A/a_0|$ vs. x illustrating the nonlinear development of a pair of helical modes with $St = 0.4$ with initial amplitudes $a_0 = 130$, 260. —○—, linear approximation.

that the nonlinear effect might not entirely negligible. With nonlinearity included, the apparent neutral (i.e. peak) position shifts downstream. The linear approximation would underestimate the peak amplitude. The linear and nonlinear solutions for the amplitude A are used in (5.22) to calculate the Mach waves in the far field. The pressure contours are illustrated in figure 10. As might be expected on the basis of the result shown in figure 9, the Mach waves are stronger than if nonlinearity is ignored, and the beam appears slightly broader.

The second case is for a pair of helical modes with $St = 0.4$, whose evolution is governed by (5.36) with $\partial/\partial\bar{t} = 0$. The equation is solved using a sixth-order predictor–correct scheme, and the solutions corresponding to different initial amplitude a_0 are shown in figure 11. The Landau coefficient is now found to have a negative real

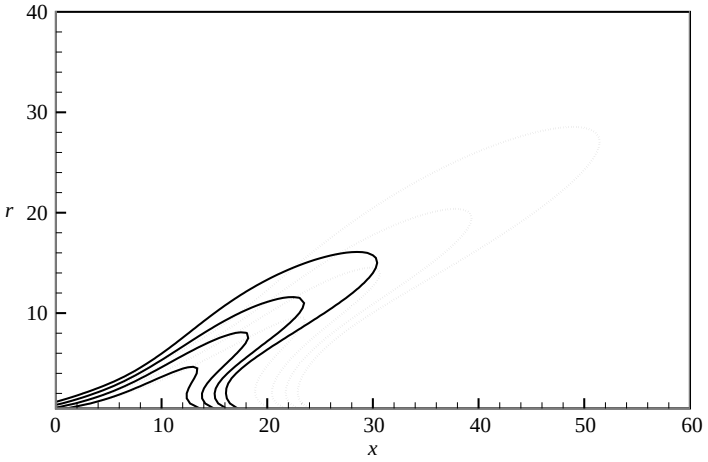

FIGURE 12. Pressure contours of the Mach waves radiated by a pair of helical modes with $St = 0.4$, predicted by (5.22) using the nonlinear solution (——) and linear approximation (· · · · · ·) for A.

part so that nonlinearity is stabilizing. The apparent neutral (peak) position of the amplitude shifts upstream. Ignoring nonlinearity would result in an overestimate of the peak amplitude. Nonlinearity become appreciable when $a_0 \sim 100$. This is found to correspond to 2.3% peak density fluctuation, or 3% peak mass-flux fluctuation, comparable with the fluctuations in the experiments of Troutt & McLaughlin (1982). It seems that the nonlinear effect might be present. However, the disturbances in the experiments had a narrow finite bandwidth, for which the nonlinear effect comes into play at a higher threshold (see the result in figure 14 below). Therefore it is highly likely that the helical modes in the experiments evolved linearly.

The Mach wave fields, calculated by using the linear and nonlinear solutions for A, are shown in figure 12. The two sets of contours have broadly similar geometric character. But inclusion of the nonlinear effect leads to a weaker Mach wave field, and a slightly more focused beam. The contour pattern corresponding to the linear solution A is representative of small-a_0 cases, and it bears a close resemblance to figure 29(b) of Troutt & McLaughlin (1982). Specifically, the angle between the beam and the downstream direction agrees with the observed value of 34°.

Finally, we consider the Mach waves radiated by modulated wavetrains (or wavepackets). The evolution of the latter is described, in the spectral space, by (5.37) subject to (5.39). The system is solved using a sixth-order predictor–corrector scheme. The integrals are evaluated using Simpson's rule. To avoid evaluating a triple integral at each step, we note that D, defined by (5.38), obeys the recurrence relation

$$\widehat{D}(\bar{x}, \tilde{\omega}_1, \tilde{\omega}_2) = \widehat{D}(\bar{x} - 2\delta\bar{x}, \tilde{\omega}_1, \tilde{\omega}_2)\, \mathrm{e}^{-2(\mathrm{i}\tilde{\omega}_1/c)\delta\bar{x}} + \frac{\delta\bar{x}}{3} \sum_{n=0}^{2} q_n \widehat{A}(\bar{x} - n\delta\bar{x}, \tilde{\omega}_2) \widehat{A}^*(\bar{x} - n\delta\bar{x}, \tilde{\omega}_2 - \tilde{\omega}_1)\, \mathrm{e}^{-n(\mathrm{i}\tilde{\omega}_1/c)\delta\bar{x}},$$

where $\delta\bar{x}$ is the step size, $q_0 = q_2 = 1$ and $q_1 = 4$ are parameters in Simpson's rule. The initial spectrum $a_s(\tilde{\omega})$ is taken to be given by (3.32), which mimics the measured spectra in figure 16 of Troutt & McLaughlin's (1982). Figure 13 shows how the spectrum evolves nonlinearly. It more or less retains its initial symmetric

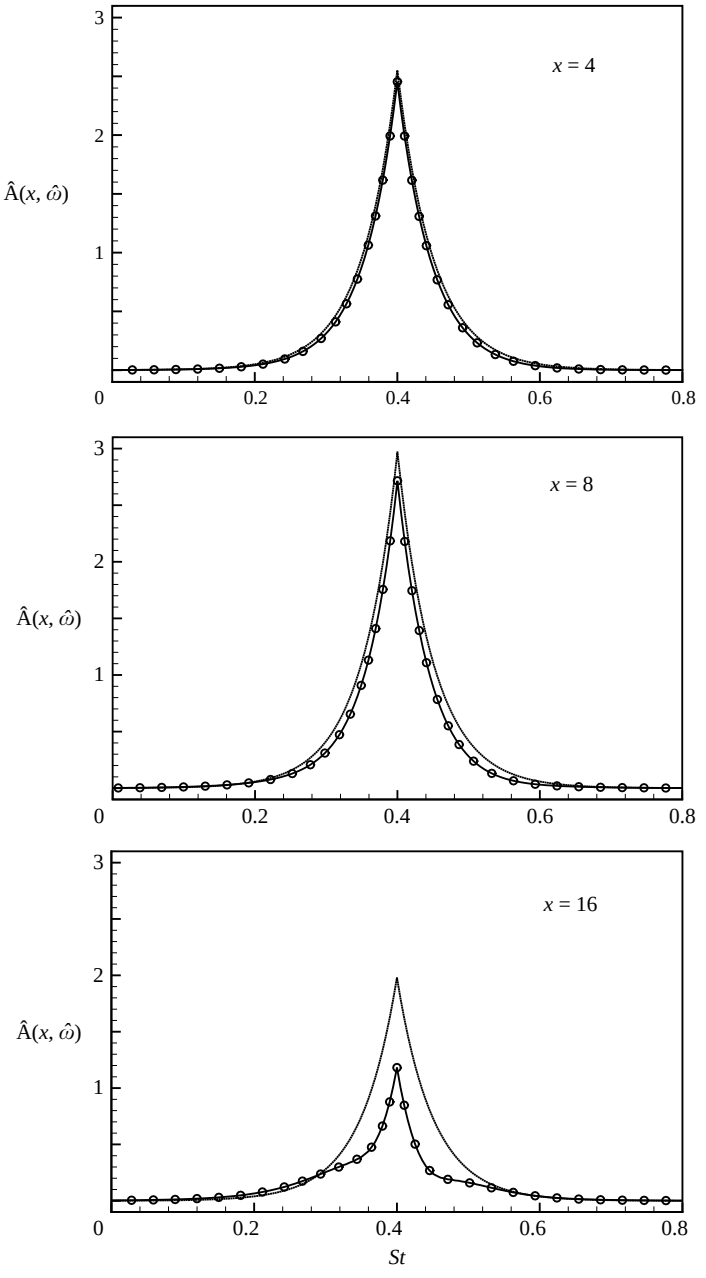

FIGURE 13. Nonlinear development of the spectrum of a wavetrain with frequencies centred at $St = 0.4$. Parameters: $\Delta^{-1} = 0.16$, $a_0 = 1300$.

shape in the linear stage. At the late stage ($x = 16$), the components in the lower-frequency sideband overtake those in the higher-frequency sideband, consistent with the experimental observation. The stabilizing effect of nonlinearity is reflected in the spectral development. The time-averaged acoustic power is shown in figure 14 for different a_0, which measures the initial overall amplitude of the wavetrain. Interestingly, a wavetrain is much less sensitive to nonlinearity than a single wave in

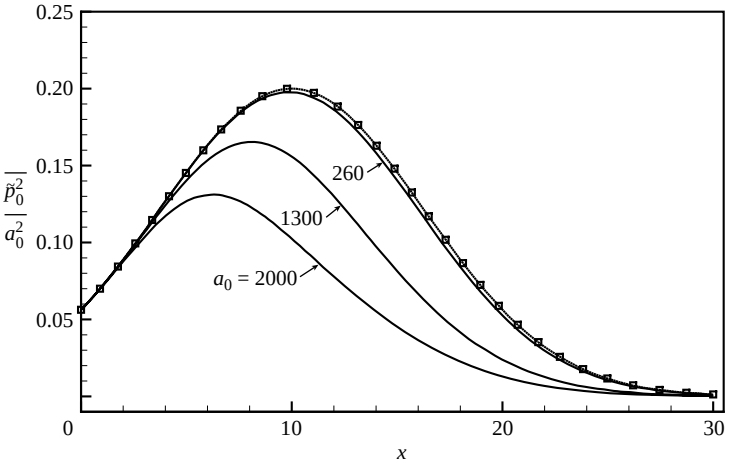

FIGURE 14. $\overline{\tilde{p}_0^2}/a_0^2$ vs. x illustrating the nonlinear development of a wavetrain with an initial amplitudes $a_0 = 260$, 1300 and 2600.

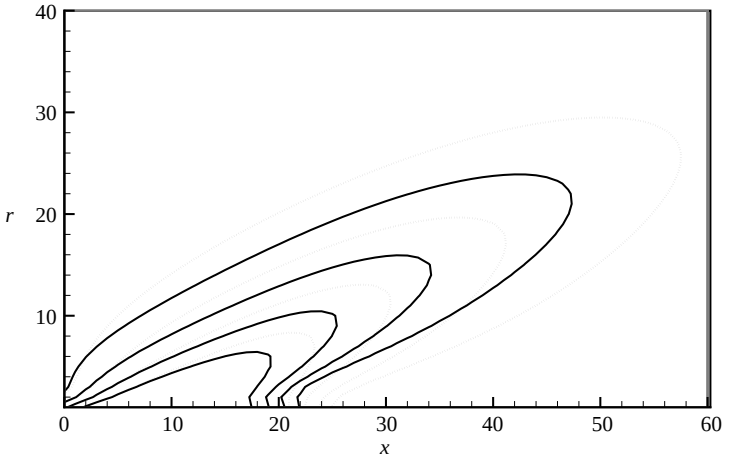

FIGURE 15. Pressure contours of the Mach waves radiated by a wavetrain ($St = 0.4$, $a_0 = 1300$), predicted by (5.25), using the nonlinear solution (——) and linear approximation (· · · · · ·) for A.

the sense that the threshold magnitude for the nonlinear effect to become appreciable is larger. As is shown in figure 14, the wavetrain (with $\Delta^{-1} = 0.16$) evolves almost linearly for $a_0 = 260$, but for a single wave (which corresponds to $\Delta^{-1} = 0$), the nonlinear effect is already significant when $a_0 = 130$. Using the nonlinear solution for $\widehat{A}(\bar{x}, \tilde{\omega})$ in (5.25), we obtain the Mach wave field shown in figure 15. For comparison, the Mach wave field predicted by using a linear approximation for A is also included. Comparing with the respective counterparts for a simple wave shown in figure 12, one notes that the Mach wave beam radiated by a wavetrain is broader. Nonlinearity has a similar effect as for a single wave (cf. figure 12): it reduces the emission and but renders the beam more focused. For the symmetric mode with $St = 0.4$ or the helical modes with $St = 0.2$, the effect of nonlinearity would be opposite because the Landau coefficients have positive real parts.

7. Summary and conclusion

In this paper, a self-consistent mathematical description is presented for the Mach wave radiation by nonlinearly evolving supersonic instability wavetrains, which is one of the fundamental noise-generation mechanisms in a supersonic jet. Using matched asymptotic expansion and multiple-scale techniques, we derive appropriate amplitude equations for the distinguished regime in which nonlinearity and non-parallelism are both important.

It is shown that the energy of the radiated Mach waves concentrates in a highly directional beam, which is a distinctive feature of supersonic jet noise. The intrinsic orientation of the beam is found to be a function of the phase speed of the instability mode and the jet Mach number based on the ambient sound speed. In the case of a planar or circular jet, the beam is perpendicular to the Mach wave fronts. The Mach wave beam consists of two asymptotic regions: a near field and a far field. In each of these the solution for the acoustic pressure was expressed explicitly in terms of the amplitude function of the instability wavetrain, thereby offering useful analytical insights into the radiation process. It must be pointed out that the analysis and the solutions for the Mach waves, as presented in § 4 and § 5.2, are in fact valid for an instability wavetrain modulated on arbitrary time and legnth scales (provided that they are longer than the period and wavelength of the carrier wave respectively).

Comparisons with DNS and relevant experimental data show that the present theory can successfully reproduce the most salient qualitative features of the Mach wave field. A good degree of quantitative agreement was noted as well.

As was indicated in the Introduction, the nonlinear evolution of the instability wavetrains may take different routes and therefore requires different nonlinear theories depending on the size of their initial amplitude. The amplitude equations in the present theory apply only to quite weak disturbances, which evolve on the $O(R^{1/2})$ length scale. In flows of typical technological interest, disturbances of larger amplitude are likely to arise, and it is important to consider the radiation properties of stronger wavetrains. Their nonlinear evolution occurs over much shorter length scale than that considered here, and may be described by non-equilibrium critical-layer dynamics. Specifically, for helical modes if their amplitude rises to $O(R^{-1})$, the non-equilibrium effect becomes important (whereas non-parallelism becomes secondary). When ϵR is below a critical value, the modes go through nonlinear amplification followed by exponential decay (Wu *et al.* 1993). In this case, the radiated Mach wave remains being described by the solution given in § 5.2 on the understanding that $\bar{x} = R^{-1/3}$, $\bar{r} = R^{-1/3} r$, $\tilde{r} = R^{-2/3} r$, and A satisfies the amplitude equation in Wu *et al.* (1993). However, once ϵR exceeds the critical value, the amplitude develops a singularity at a finite distance downstream. Predicting the continued nonlinear evolution of the instability modes and the Mach wave radiation then becomes a major challenge because the removal of the singularity requires consideration of the fully nonlinear Euler equations (Goldstein & Choi 1989).

It may be note that the threshold amplitide of $O(R^{-1})$ for the non-equlibrium regime is higher than that for the equilibrium regime by a factor $O(R^{-1/6})$, which would be 10 for typical $R \approx 10^6$ that may be encountered in technological applications. This disparity suggests that there exists a sizable range of disturbance amplitude to which the present theory applies. From the practical point of view, it may be worthwhile to construct a composite solution or evolution equation, which includes both the non-equilibrium and non-parallel effects. This would not only help quantify the relative role of these two factors, but also would lead to a more precise identification of the critical amplitude above which the finite-distance singularity develops.

The author would like to thank Professors H. Zhou, J. Luo and W. Cao (Tianjin University, China) and Dr M. Choudhari (NASA Langley Research Center) for helpful discussions.

REFERENCES

Avital, E. J., Sandham, N. D. & Luo, K. H. 1998 Mach wave radiation by mixing layers. Part I: Analysis of the sound. Part II: Analysis of the source field. *Theor. Comput. Fluid Dyn.* **12**, 73–108.

Bishop, K. A., Ffowcs Williams, J. E. & Smith, W. 1971 On the noise sources of the unsuppressed high-speed jet. *J. Fluid Mech.* **50**, 21–31.

Cowley, S. J. & Wu, X. 1994 Asymptotic approaches to transition modelling. In *Progress in Transition Modelling*, *AGARD Rep.* 793.

Crighton, D. G. & Huerre, P. 1990 Shear-layer pressure fluctuations and superdirective acoustic sources. *J. Fluid Mech.* **220**, 355–368.

Crow, S. C. 1970 Aerodynamic sound emission as a singular perturbation problem. *Stud. Appl. Maths* **49**, 21–44.

Crow, S. C. & Champagne, F. H. 1971 Orderly structure in jet turbulence. *J. Fluid Mech.* **48**, 547–591.

Ffowcs Williams, J. E. & Maidanik, G. 1965 The Mach wave field radiated by supersonic turbulent shear flows. *J. Fluid Mech.* **21**, 641–657.

Freund, J. B., Lele, S. K. & Moin, P. 2000 Numerical simulation of a Mach 1.92 turbulent jet and its sound field. *AIAA J.* **38**, 2023–2031.

Goldstein, M. E. 1994 Nonlinear interactions between oblique instability waves on nearly parallel shear flows. *Phys. Fluids* A **6**, 724–735.

Goldstein, M. E. 1995 The role of nonlinear critical layers in boundary-layer transition. *Phil. Trans. R. Soc. Lond.* A **352**, 425–442.

Goldstein, M. E. & Choi, S.-W. 1989 Nonlinear evolution of interacting oblique waves on two-dimensional shear layers. *J. Fluid Mech.* **207**, 97–120, and Corrigendum, *J. Fluid Mech.* **216**, 1990, 659–663.

Goldstein, M. E. & Leib, S. J. 1989 Nonlinear evolution of oblique waves on compressible shear layers. *J. Fluid Mech.* **207**, 73–96.

Howe, M. S. 1975 Contributions to the theory of aerodynamics sound, with application to excess jet noise and the theory of the flute. *J Fluid Mech.* **71**, 625–673.

Jackson, T. L. & Grosch, C. E. 1989 Inviscid spatial stability of a compressible mixing layer. *J. Fluid Mech.* **208**, 609–637.

Kambe, T. 1986 Acoustic emission by vortex motions. *J. Fluid Mech.* **173**, 643–666.

Khavaran, A., Bridges, J. & Freund, J. B. 2002 A parametric study of fine-scale turbulence mixing noise. *AIAA Paper* 2002–2419.

Kinzie, K. W. & McLaughlin, D. K. 1995 Aeroacoustic properties of supersonic elliptic jets. *J. Fluid Mech.* **395**, 1–28.

Leib, S. J. 1991 Nonlinear evolution of subsonic and supersonic disturbances on a compressible free shear layer. *J. Fluid Mech.* **224**, 551–578.

Leib, S. J. & Lee, S. S. 1995 Nonlinear evolution of a pair of oblique instability waves in a supersonic boundary layer. *J. Fluid Mech.* **282**, 339–371.

Lighthill, M. J. 1952 On sound generated aerodynamically. *Proc. R. Soc. Lond.* A **211**, 564–587.

Lighthill, M. J. 1954 On sound generated aerodynamically. II. Turbulence as a source of sound. *Proc. R. Soc. Lond.* A **222**, 1–32.

Lilley, G. M. 1974 On the noise from jets, noise mechanisms. *AGARD-CP*-131, pp. 13.1–13.12.

Lowson, M. V. & Ollerhead, J. B. 1968 Visualization of noise from cold supersonic jets. *J. Acoust. Soc. Am.* **44**, 624–630.

Luo, K. H. & Sandham, N. D. 1997 Instability of vortical and acoustic modes in supersonic jets. *Phys. Fluids* **9**, 1003–1013.

McLaughlin, D. K., Morrison, G. L. & Troutt, T. R. 1975 Experiments on the instability waves in a supersonic jet and their acoustic radiation. *J. Fluid Mech.* **69**, 73–95.

Mitchell, B. E., Lele, S. J. & Moin, P. 1997 Direct computation of Mach wave radiation in an axisymmetric supersonic jet. *AIAA J.* **35**, 1574–1580.

Mohseni, K., Colonius, T. & Freund, J. B. 2002 An evaluation of linear instability waves as sources of sound in a supersonic turbulent jet. *Phys. Fluids* **14**, 3593–3600.

Oertel, H. 1979 Mach wave radiation of hot supersonic jets. In *Mechanics of Sound Generation in Flows* (ed. E. A. Muller), pp. 275–281. Springer.

Panda, J. & Seasholtz, R. G. 2002 Experimental investigation of density fluctuations in high-speed jets and correlation with generated noise. *J. Fluid Mech.* **450**, 97–130.

Phillips, O. M. 1960 On the generation of sound by supersonic turbulent shear layers. *J. Fluid Mech.* **9**, 1–27.

Stewartson, K. & Stuart, J. T. 1971 A nonlinear instability theory for a wave system in plane Poiseuille flow. *J. Fluid Mech.* **48**, 529–545.

Tam, C. K. W. 1971 Directional acoustic radiation from a supersonic jet generated by shear layer instability. *J. Fluid Mech.* **46**, 757–768.

Tam, C. K. W. 1972 On the noise of a nearly ideally expanded supersonic jet. *J. Fluid Mech.* **51**, 69–95.

Tam, C. K. W. 1995 Supersonic jet noise. *Annu. Rev. Fluid Mech.* **27**, 17–43.

Tam, C. K. W. & Burton, D. E. 1984*a* Sound generated by instability waves of supersonic flow. Part 1. Two dimensional mixing layers. *J. Fluid Mech.* **138**, 249–271.

Tam, C. K. W. & Burton, D. E. 1984*b* Sound generated by instability waves of supersonic flow. Part 2. Axisymmetric jets. *J. Fluid Mech.* **138**, 273–295.

Tam, C. K. W., Chen, P. & Seiner, J. M. 1992 Relationship between instability waves and noise of high-speed jets. *AIAA. J.* **30**, 1747–1752.

Tam, C. K. W. & Hu, F. 1989 On the three families of instability waves of high-speed jets. *J. Fluid Mech.* **201**, 447–483.

Tam, C. K. W. & Morris, P. J. 1980 The radiation of sound by the instability waves of a compressible plane turbulent shear layer. *J. Fluid Mech.* **98**, 349–381.

Troutt, T. R. & McLaughlin, D. K. 1982 Experiments on the flow and acoustic properties of a moderate-Reynolds-number supersonic jet. *J. Fluid Mech.* **116**, 123–156.

Wu, X., Lee, S. S. & Cowley, S. J. 1993 On the weakly nonlinear three-dimensional instability of shear flows to pairs of oblique waves: the Stokes layer as a paradigm. *J. Fluid Mech.* **253**, 681–721.